The *Drosophila* hematopoietic niche assembles through collective cell migration controlled by neighbor tissues and Slit-Robo signaling

Kara A. Nelson[1,2], Kari F. Lenhart[3], Lauren Anllo[1,2], Stephen DiNardo[1,2]

[1]Department of Cell and Developmental Biology, Perelman School of Medicine at the University of Pennsylvania, 421 Curie Blvd. Philadelphia, PA 19104, United States

[2]Institute for Regenerative Medicine at the University of Pennsylvania, 3400 Civic Center Blvd. Philadelphia, PA 19104, United States

[3]Department of Biology, Drexel University, 3245 Chestnut St. Philadelphia, PA 19104, United States

knelson7@pennmedicine.upenn.edu https://orcid.org/0000-0003-4847-2835

kfl36@drexel.edu https://orcid.org/0000-0003-4575-5514

anllol22@ecu.edu https://orcid.org/0000-0001-5482-5882

sdinardo@pennmedicine.upenn.edu https://orcid.org/0000-0003-4131-5511

Impact Statement

A new example of niche formation is provided which reveals the mode of niche cell migration, implicates extrinsic sources that deliver positional information, and uncovers the signaling pathway required for the precise, stereotypical positioning of the niche.

Abstract

Niches are often found in specific positions in tissues relative to the stem cells they support. Consistency of niche position suggests that placement is important for niche function. However, the complexity of most niches has precluded a thorough understanding of how their proper placement is established. To address this, we investigated the formation of a genetically tractable niche, the *Drosophila* Posterior Signaling Center (PSC), the assembly of which had not been previously explored. This niche controls hematopoietic progenitors of the lymph gland (LG). PSC cells were previously shown to be specified laterally in the embryo, but ultimately reside dorsally, at the LG posterior. Here, using live-imaging, we show that PSC cells migrate as a tight collective and associate with multiple tissues during their trajectory to the LG posterior. We find that Slit emanating from two extrinsic sources, visceral mesoderm and cardioblasts, is required for the PSC to remain a collective, and for its attachment to cardioblasts during migration. Without proper Slit-Robo signaling, PSC cells disperse, form aberrant contacts, and ultimately fail to reach their stereotypical position near progenitors. Our work characterizes a novel example of niche formation and identifies an extrinsic signaling relay that controls precise niche positioning.

Introduction

Homeostasis and repair of many organs relies on a resident stem cell population. Stem cell behavior is often coordinated by a niche (Morrison & Spradling, 2008)—the specific microenvironment that contains stem cells—and abnormal regulation can severely impact health by leading to tissue atrophy or tumor formation (Chakkalakal et al., 2012; Ferraro et al., 2010; Kobielak et al., 2007; Walkley et al., 2007). Thus, it is essential to understand stem cell-niche interactions. An important step in understanding the behavior of a mature niche is understanding the particular attributes it acquires—such as cellular features and the positioning of its cells with respect to each other and stem cells—and how those attributes are regulated as the niche is built during development. Yet, there are very few studies of niche formation at the cellular level. The few well-studied niches consistently acquire tissue-specific positional and structural characteristics (Anllo et al., 2019; Biggs et al., 2018; Gordon et al., 2020; Sumigray et al., 2018). The reproducibility of these characteristics suggests that acquisition of a particular architecture is essential to niche function and emphasizes the importance of understanding how the architecture of a given niche is established.

Frequent barriers to studying niche formation include niche complexity and lack of niche cell markers (Heitman et al., 2018; Pinho & Frenette, 2019). Studying niche formation *in vivo* is further hindered by an inability to follow its constituent cells as they form the niche in real-time due to lack of tissue and organism transparency, and the existence of large-scale tissue movements (Bostock et al., 2020; Boulais & Frenette, 2015; Gregg & Butcher, 2012). The mammalian hematopoietic stem cell niche is a prime example of a difficult-to-study niche due to its location within opaque bone and its complexity—it is comprised of numerous cellular components and molecular factors (Boulais & Frenette, 2015; Calvi et al., 2003; Pinho & Frenette, 2019; Zhang et al., 2003). Despite these limitations, some niches, such as the mammalian intestinal epithelium and hair follicle, are beginning to be studied at the cellular level (Anllo & DiNardo, 2022; Díaz-Torres et al., 2021; Gupta et al., 2019; Pentinmikko et al., 2022; Sumigray et al., 2018). However, investigations about establishment of these well-characterized niches still suffer from challenges including limited real-time imaging and lack of tissue-specific manipulations.

To overcome these limitations and gain insight into the mechanisms that drive niche formation, we have investigated the development of the niche that supports the *Drosophila* larval hematopoietic organ: the lymph gland (LG). The cells that constitute this niche, called the posterior signaling center (PSC), and the markers that label it are known (Crozatier et al., 2004; Lebestky et al., 2003; Mandal et al., 2007). Additionally, the PSC resides under a thin epidermal covering, making it amenable to live-imaging with high spatial resolution, as we show here. The dynamic information afforded by live-imaging can reveal the mechanism of migration and implicate nearby tissues as a source for guiding signals. These advantages, paired with facile *Drosophila* genetics, make for a powerful experimental system in which PSC formation can be visualized *in vivo* and the underlying mechanisms probed.

Minimal information exists about the formation of the PSC, as most analyses of the lymph gland have focused on the steady-state operations of late larval stages when the gland is mature and most accessible due to its larger size. While the mature LGs are comprised of multiple pairs of lobes (Koranteng et al., 2022; SHRESTHA & GATEFF, 1982), we use 'lymph gland' to refer to only one of the pair of thoroughly characterized, bilaterally symmetric 'primary' lobes. In late larval stages the LG contains thousands of cells, organized into multiple zones: the medullary, intermediate, and cortical zones, and the PSC (Banerjee et al., 2019; Jung et al., 2005; Lanot et al., 2001). The PSC regulates the adjacent hematopoietic progenitors of the medullary zone; these progenitors are progressively differentiated from the innermost region of the LG, radially outward (Cho et al., 2020; Jung et al., 2005; Luo et al., 2020; Mandal et al., 2007). The mature, terminally differentiated hemocytes reside at the outermost cortex of the gland, in the cortical zone, and between these zones are the cells of the intermediate zone (Jung et al., 2005; Krzemien et al., 2010; Spratford et al., 2021). Recent scRNA-seq analyses have identified new types of hemocytes in the LG (Cho et al., 2020; Girard et al., 2021), but the three main

types are analogous to vertebrate myeloid cells and include crystal cells, plasmatocytes, and lamellocytes, which are responsible for wound healing and innate immunity (Banerjee et al., 2019; Lanot et al., 2001; Rizki & Rizki, 1992).

The larval PSC facilitates wound repair, immune response, and homeostasis and does so by performing two key functions: maintaining progenitors and inducing progenitor differentiation (Baldeosingh et al., 2018; Crozatier et al., 2004; Krzemień et al., 2007; Mandal et al., 2007; Ramesh et al., 2021). PSC positioning is such that it contacts both the least differentiated progenitors and mature hemocytes (Baldeosingh et al., 2018; Jung et al., 2005), a seemingly prime location where the PSC is poised to both implement regulation and receive feedback, thereby maintaining homeostasis in the LG. For example, upon immune challenge, the PSC senses and responds to the threat by instructing differentiation of progenitors (Khadilkar et al., n.d.; Louradour et al., 2017; Sinenko et al., 2012). The PSC engages multiple signaling pathways to execute its roles and relies on cell biological characteristics of its component cells, such as occluding or gap junctions, to do so (Baldeosingh et al., 2018; Ho et al., 2023; Khadilkar et al., 2017; Mandal et al., 2007; Sinenko et al., 2009).

PSC functionality is integral for organism health, as PSC loss can cause precocious differentiation of progenitors under homeostatic conditions and inability to produce lamellocytes under immune challenge conditions (Baldeosingh et al., 2018; Krzemień et al., 2007; Mandal et al., 2007). PSC-regulated homeostatic maintenance of the larval LG is crucial, as the LG will ultimately rupture, releasing its constituents into circulation to contribute to the hematopoietic pool in pupal and adult stages (Grigorian et al., 2011; Holz et al., 2003). Furthermore, recent publications suggest that the PSC itself adopts new functions upon LG rupture – PSC cells become highly motile and phagocytic and are capable of transdifferentiating into lamellocytes or plasmatocytes upon immune challenge (Boulet et al., 2021; Hirschhäuser et al., 2023).

Though the late larval PSC is comprised of about 30-50 cells (Ho et al., 2021; Morin-Poulard et al., 2016; Tokusumi et al., 2015), it is initially specified as only about five cells (Mandal et al., 2007). The expansion of PSC cell number takes place only after the five cells become organized into the PSC at the posterior of the developing LG during late stages of embryogenesis (Mandal et al., 2007). How the PSC becomes consistently positioned after specification is unknown and is our focus here. The LG itself is specified about mid-way through embryogenesis, around stage 12, from cardiogenic mesoderm as three cell clusters located laterally—one in each thoracic segment (schematized in Figure 1A, left; Crozatier et al., 2004; Mandal et al., 2004, 2007). The PSC is specified from the posterior-most LG cells by expression of Antennapedia and the silencing of Homothorax (Mandal et al., 2007). A transcription factor, Collier, the *Drosophila* ortholog of mammalian early B-cell factor, is initially expressed in the entire LG primordium but becomes restricted to the PSC and is necessary for its maintenance and function (Crozatier et al., 2004; Krzemień et al., 2007). From fixed preparations, its known that the three LG clusters coalesce along the anterior-posterior axis before reaching the dorsal midline. At the end of embryogenesis, the cluster of PSC niche cells resides at the posterior of each bilaterally symmetric lymph gland; each gland flanks the dorsal vessel—the *Drosophila* heart—at the dorsal midline (schematized in Figure 1A, right; (Crozatier et al., 2004; Mandal et al., 2007). Apart from this description nothing is known about how the PSC is built, and no live-imaging of the PSC has been conducted during embryogenesis. Despite the probable importance of PSC positioning to later function, the mechanism of migration, the signals guiding migration, and interactions among constituent cells—each integral aspects of organogenesis—are entirely unknown.

We have conducted the first *in vivo* live-imaging of PSC formation, visualizing migration of PSC cells from their origin, lateral in the embryo, to their final, dorsal position at the posterior of the LG. We find that a prominent, regulated feature of this niche is the migration of its constituent cells as a collective. Live-imaging also revealed neighboring tissues that could feasibly signal to influence PSC migration as well as its positioning in the LG. Using genetic ablation and mutant analyses, we have identified that both the dorsal vessel and visceral mesoderm are required for proper positioning of the PSC. In addition, mutant analyses and tissue-specific

challenges revealed an intricate web of Slit-Robo signaling in and between these tissues that is essential to establish positioning of PSC cells as a coalesced, compact collective at the LG posterior. Finally, we use live-imaging to show that Slit signaling is essential to maintain collectivity of PSC cells and properly position these cells during their migration. Taken together, we have uncovered a new example of collective cell migration, revealed some of its mechanistic underpinnings, and implicated a signaling relay required to properly build and position this niche.

Results

Live-imaging reveals dynamics of PSC formation.

While PSC formation is undoubtedly a dynamic process, current knowledge in the field is derived exclusively from static timepoints using fixed embryos (Figure 1A). Thus, we sought to visualize the entirety of PSC migration in real time. To identify and track PSC cells live, we first confirmed their location at various time points in fixed embryos using the accepted markers, Antp and Odd, where co-expression demarcates PSC cells. We characterized PSC positioning in stages ranging from migration onset, stage 14, until migration completion, stage 16 (schematized in Fig 1B'-F'). Prior to migration, the PSC appeared as a compact cluster of cells (Figure 1B, green underline), it appeared more elongated through mid-migration (Figure 1C-1E), and ultimately it assumed a compact, clustered organization at the posterior of the lymph gland (Figure 1F). During migration and upon its completion, the PSC flanked Antp+ cardioblasts of the dorsal vessel (Figure 1F, brackets). Though not explored further here, ECM components, Perlecan and Viking, were expressed around the PSC collective including between the PSC and the adjacent cardioblasts (Figure S1A and S1B).

To our knowledge, a sufficiently bright, stable marker that labels only PSC cells during migration stages does not exist. Thus, for live-imaging we combined Hand-RFP, which marks lymph gland (including the PSC) and cardioblasts, with a myristoylated GFP driven by Antp-GAL4 (Antp > myrGFP) to mark the PSC but not other lymph gland cells (Figure 1G-J). We performed timelapse imaging on embryos beginning after PSC specification (stage 13) until the PSC completed migration and morphogenesis (stage 17). We observed that the PSC moved as a collective for the entire migration (Figure 1G). During migration many PSC cells extended protrusions—some reached far anteriorly, encasing the lymph gland (Figure 1H', bracket) while others were shorter or branched (Figure 1H''', arrowheads). The protrusions exhibited no apparent directional bias but were more common at non-dorsal vessel-adjacent surfaces of the collective. During migration some cells shifted positioning with respect to one another. For example, two lateral PSC cells that abut early on (Figure 1I, 0m, arrowhead) become separated by interdigitating cells (Figure 1I, 8-40m, magenta and green dots). In general, however, most cells remained at relatively fixed positions within the collective—particularly the posterior-most, dorsal vessel-adjacent PSC cells (Figure 1I, orange dots and Figure 1G, arrowheads). Live-imaging revealed the importance of collective migration in building this niche, even as some PSC cells exhibit cellular extensions and shift position within the collective.

Visceral, cardiac, and alary muscles are near the PSC throughout its migration.

Crucially, live-imaging also uncovered that the PSC was within signaling distance of various muscles for the entirety of its migration. It is well-documented that muscles can supply positional information to nearby tissues (Anllo & DiNardo, 2022; Lucila Scimone et al., 2017; Witchley et al., 2013), and our imaging indicated that visceral muscle (or, visceral mesoderm; Vm) and cardioblasts (CBs) of the dorsal vessel were each near the PSC. We live-imaged with a dorsolateral vantage point which revealed that the PSC migrated dorsally in synchrony with CBs and Vm (Figure 1J). The PSC remained laterally affixed to Antp+ CBs (Figure 1J', blue) and slightly dorsal to Antp+ Vm (Figure 1J', orange) throughout migration.

Based on segmental positioning, we suspected the PSC was also near alary muscle (AM)—segmentally repeating muscles that attach internal organs to the body wall. We live-imaged PSC and AM migration from a dorsal vantage point with Antp>CD8:GFP and *org-1*-HN39::RFP, a marker with expression restricted to AMs.

171 Indeed, the first AM was immediately lateral to the PSC for the entirety of their synchronized migration to the
172 dorsal midline (Figure 1K, PSCs outlined in green). We confirmed this proximity by fixing *org-1*-HN39::RFP
173 embryos and staining for Antp, which revealed that at late stages, the A1 AM ensheathed the PSC (Figure S1D),
174 with some fibers encasing individual PSC cells (Figure S1E).

175 Thus, live-imaging provided invaluable insights, advancing our knowledge of PSC formation from that
176 attainable through analysis of fixed preparations (Figure 1A), by revealing the mode of PSC migration and the
177 spatiotemporal dynamics of the PSC relative to nearby tissues (Figure 1L). The sustained proximity of alary
178 muscles, visceral mesoderm, and cardioblasts to the PSC made each a strong candidate for influencing PSC
179 positioning.

180 **Vm and CBs are required for proper PSC positioning.**

181 Having identified multiple candidates, we next investigated whether any or all of these muscles were necessary
182 for proper PSC positioning. To test a role for AM, we ablated it by expressing the pro-apoptotic factor, *grim*,
183 using the AM-specific AME_r-GAL4. Ablation was successful, evidenced by lack of GFP-labeled AMs (Figure 2B)
184 compared to controls (Figure 2A). Based on our characterization of the wildtype PSC (Figure 1), we developed
185 criteria to score PSCs at the culmination of their migration as positioned 'normally' or 'abnormally'. A 'normal'
186 PSC must be 1) coalesced within one nuclear diameter of one another, 2) adjacent to the dorsal vessel, and 3)
187 at the same dorsal-ventral position as the posterior-most progenitors of the lymph gland. Surprisingly, AM
188 ablation had no impact on PSC positioning (Figure 2C) nor the total number of PSC cells (Figure S2A), indicating
189 that AMs are not required for proper PSC formation.

190 To determine whether Vm was involved in forming the PSC, we examined *biniou* mutants in which the Vm is
191 genetically ablated (Zaffran et al., 2001). In controls, the Vm is apparent at stage 12 as columnar, Fas3+ cells
192 (Figure 2D, brackets). By stage 16, Vm has surrounded the gut and constricted it into sections (Figure 2E, arrow
193 is first Vm constriction that separates the first two gut sections). By contrast, in *bin* mutants, minimal Fas3+ Vm
194 was detected at stage 12 (Figure 2G), and it was absent at stage 16 (Figure 2H). The majority of bin^{R22} mutants
195 and bin^{R22}/ bin^{S4} transheterozygous mutants had abnormal PSC positioning (Figure 2I, arrowheads) compared
196 to heterozygote controls with normal PSC positioning (Figure 2F, outlines; quantified in 2J). We detected no Bin
197 protein in PSC cells (Figure S2B), indicating PSC positioning defects in *bin* mutants did not originate PSC-
198 intrinsically but rather were caused by lack of Vm.

199 To confirm a role for Vm in PSC formation, we ablated Vm by expressing the proapoptotic gene, *hid,* using a
200 Vm-specific driver, bap-GAL4. Stage 11 sibling controls displayed characteristic organization of Vm precursors
201 (Figure 2K): segmentally repeating mounds of fusion competent myoblasts (FCMs; between green and
202 magenta lines) atop columnar founder cells (FCs; below magenta line). Stage 11 ablated embryos were largely
203 missing FCMs (Figure 2N, brackets). Though most FCs were present at this stage, they exhibited substantially
204 reduced Bin expression compared to controls (Figure S2C and S2D, quantified in S2E), suggesting improper
205 differentiation. By stage 16 no Vm was detectable (Figure 2O). Vm-ablated embryos had abnormal PSC
206 positioning (Figure 2P, arrowheads) more often than sibling controls (Figure 2M, quantified in 2Q). Taken
207 together, these analyses definitively establish that an extrinsic cue(s) provided by Vm governs PSC positioning.

208 To address when the cue might be delivered, we analyzed *jelly belly* mutants and *bagpipe* hypomorphs, bap^{208}.
209 In both backgrounds Vm precursors are present initially at stage 11 but do not differentiate or migrate properly
210 from stages 13-16 (Figure S2F-S2J and Englund et al., 2003; Lee et al., 2003; Weiss et al., 2001). In both
211 mutants PSC positioning was unaffected (Figure S2K, N, and P; quantified in S2L and S2Q), revealing that early
212 signaling from Vm is sufficient for PSC positioning.

213 Finally, to assess whether cardioblasts of the dorsal vessel impact PSC positioning, we expressed *hid* or *grim*
214 with the CB-specific driver, tinCΔ4-GAL4. We used conditions that restricted defects to CBs and left Vm
215 unaffected (see Materials and Methods). Whereas controls had uninterrupted strings of Mef2-labeled CBs

(Figure 2R), the manipulated embryos had significant dorsal vessel ablation, evident by gaps in CBs (Figure 2S, bracket). We elected to analyze stage 14 and 15 embryos because these presented with appreciable ablation over larger distances compared to stage 16 onwards. Oftentimes both sides of the bilaterally symmetric dorsal vessel were ablated; sometimes only one side was ablated. For a given instance of dorsal vessel ablation, we documented whether the ipsilateral PSC was positioned normally. While the PSC occasionally appeared mis-positioned in non-ablated controls, for ablated dorsal vessel the ipsilateral PSC was mis-positioned more frequently (Figure 2T). These data suggest that dorsal vessel CBs influence PSC formation.

Slit-Robo signaling is required for proper PSC formation.

To identify a cue necessary for positioning the PSC, we sought a signal that is expressed in early Vm and/or CBs. The secreted glycoprotein Slit is known to be expressed in both tissues and has been implicated as a positional cue in multiple developmental contexts (Anllo & DiNardo, 2022; Kidd et al., 1999; Kolesnikov & Beckendorf, 2005; MacMullin & Jacobs, 2006a; Rothberg et al., 1990). We confirmed that Slit is detectable in both Vm and CBs at relatively early stages of PSC migration (Figure 3A and 3B). Importantly, *sli* mutants exhibited mis-positioned PSCs more frequently compared to controls (Figure 3A and 3B, quantified in 3E), indicating a requirement for Slit in properly positioning the PSC.

To confirm that PSC cells can respond to Slit ligand, we examined the expression of the three Robo class receptors. We found evidence for only Robo1 and Robo2 expression in the PSC (Figure S3A an S3B). Thus, to test the requirement for Robo signaling, we analyzed single and double *robo1* and *robo2* mutants. For both single mutants, about 50% of embryos had abnormal PSC positioning (Figure 3I and 3J, arrowheads). About 75% of double mutants had abnormal PSCs (Figure 3K), a frequency which matches that of *sli* mutants. These results demonstrate that Slit signaling through Robo1 and Robo2 is required for properly positioning the PSC.

Dorsal vessel-derived Slit signaling is required for PSC positioning.

To test whether CBs were a source of Slit important for PSC positioning we used tinCΔ4-GAL4 to prevent either production or release of Slit specifically from dorsal vessel using RNAi or sequestration via overexpression of the Robo1 receptor, respectively. We confirmed that two independent Slit RNAi's eliminated nearly all Slit accumulation at CBs (Figure 3O' and 3Q'), while Robo overexpression resulted in more pronounced Slit accumulation on CB membranes (Figure 3S') compared to control CBs (Figure 3M'). PSCs were abnormally positioned more frequently under all challenge conditions (Figure 3N, 3P, 3R) compared to controls (Figure 3S). Thus, Slit produced from CBs is essential to properly position the PSC.

Vm-derived Slit signaling is required for PSC positioning.

The additional requirement for Vm in PSC positioning and the presence of Slit expression in Vm suggested that Vm-derived Slit might also regulate PSC formation. To block Slit produced by Vm from signaling to PSCs, we sequestered Slit specifically in Vm using bap-GAL4 to overexpress Robo1. This manipulation prevents diffusion of Slit away from the tissue, as evidenced by distinct accumulation of Slit on Vm membranes (Figure 3Z) compared to diffuse Slit puncta in control Vm (Figure 3W). Under this condition, we indeed found that PSCs were mis-positioned significantly more often (Figure 3AA; quantified in 3BB). Taken together, these data suggest that Vm and CB-derived Slit signaling are both required for PSC positioning.

Vm influences dorsal vessel positioning.

While the data thus far supported a simple model wherein Slit secreted from Vm and CBs acts directly on Robo receptors expressed by PSC cells to influence PSC positioning, further investigation revealed a more complex situation. Autocrine Slit-Robo signaling among dorsal vessel cells is important for proper polarity and organization of the vessel (Medioni et al., 2008a; Qian et al., 2005; Santiago-Martínez et al., 2008). Intriguingly, in experiments where Slit was sequestered in Vm, we noticed defects in the organization of the cardioblasts (Figure 3AA, brackets; compare to control, 3X brackets). This suggested that signaling from Vm was required

for organizing the dorsal vessel—a possibility that had not been previously explored. To test this, we examined the dorsal vessels of *bin* mutants which lack Vm (Figure 2H). We identified multiple phenotypes, two of which we termed 'twisted' and 'sunken'; the dorsal vessel in Figure 4B exhibits both phenotypes. We scored a dorsal vessel as 'twisted' (Figure 4B, bracket) when there was an apparent kink in the vessel such that the left or right side sat directly atop the other; thus, when viewing a single z-slice, a span of contralateral CBs appear to be missing since they are displaced above or below that focal plane. We defined a sunken dorsal vessel (Figure 4B' and 4B'') as those cases where the whole dorsal vessel, or part of it, was displaced ventrally, deeper into the embryo. Such a case is evident in the Figure 4B mutant dorsal vessel, which spans 8µm of depth, compared to the sibling control dorsal vessel, which spans only 4µm. Both phenotypes were significantly more frequent in *bin* mutants compared to sibling controls (Figure 4C). Together, the dorsal vessel defects observed upon removal of the Vm or from trapping Slit on Vm cells reveal a previously unrecognized role for Vm in dorsal vessel formation.

PSC positioning requires Robo signaling in CBs and in PSCs.

Our results indicated that lack of Vm causes abnormal dorsal vessel positioning, and that the dorsal vessel is required for PSC positioning. In addition, our live-imaging revealed that some PSC cells are affixed to CBs of the dorsal vessel (Figure 1). Thus, it became important to test whether all PSC phenotypes might be 'passive', explained by PSC attachment to a malforming dorsal vessel. Alternatively, the PSC defects could reflect a requirement for Robo activation directly in PSC cells. Without a PSC-specific driver to directly test the latter, we re-examined *robo1*,*robo2* double mutants, this time including an additional marker that allowed us to observe PSC and CB defects independently and score for correlation between the two. If defective PSC positioning mostly correlated with defective CB positioning this would suggest a passive effect on PSCs by CBs of the dorsal vessel (Figure 4D, middle schematic). By contrast, if PSC cells were mis-positioned without a similarly mis-positioned CB nearby, this would suggest a requirement for intrinsic activation of Robo in PSC cells (Figure 4D, rightmost schematic).

The CB marker, *svp*-lacZ, labels two CBs in each hemisegment (Figure 4E, two hemisegments shown; Lo & Frasch, 2001). Normally, the PSC is compact and located adjacent to the compact Antp+ CBs (Figure 4E, PSCs outlined). Svp co-labels the last of the four strongly Antp+ CBs, and it labels the immediately posterior Antp- CB (Figure 4E, brackets). At the end of migration, Svp-LacZ+ CBs, like all CBs, are well-aligned with their bilaterally symmetric counterparts. Thus, including Svp-LacZ in our analysis served as a useful registration marker that afforded the ability to detect bilateral matching, as well as shifting of CBs or the PSC along the anterior-posterior axis (Figure 4E-4G, arrows indicate second set of Svp+ CBs).

In *robo1*,*robo2* double mutants, we found that mis-positioning of CBs and the ipsilateral PSC occurred more frequently compared to double heterozygotes (Figure 4H). We then further analyzed those instances of mis-positioning for whether the position of PSCs correlated with position of CBs. In about two-thirds of cases mis-positioning was correlated (Figure 4F and 4G, green arrowheads, quantified in 4I), suggesting that proper PSC positioning relies in part on proper CB positioning. However, in about one-third of cases PSC mis-positioning appeared independent of CB mis-positioning (Figure 4F and 4G, magenta arrowheads). We also observed PSC mis-positioning (Figure 4G, magenta arrowhead) when ipsilateral CBs were positioned normally (Figure 4G, brackets). These instances of non-correlation strongly suggest that Robo activation is required in PSC cells for their proper positioning.

Finally, we live-imaged *slit* mutants with Hand-RFP, Antp>myrGFP to examine the dynamics of PSC migration when signaling was compromised. In contrast to the robust collectivity noted throughout the migration of control PSCs (Figure 1G), this imaging revealed progressive deterioration of PSC integrity during migration. For instance, throughout imaging, one PSC cell (Figure 5A, cyan dot) bridged the gap between the Antp+ CBs (Figure 5A, yellow brackets, 0 min) and posteriorly-displaced CBs. Ultimately this PSC cell made aberrant contact with a CB from the contralateral side (Figure 5A, yellow dot, 70min). This region had a persistent gap,

306 possibly reflecting improper sealing of the dorsal vessel (Figure 5A, arrows, 112 min), as well as improper A-P
307 alignment of Antp+ CBs with their contralateral counterparts (Figure 5A, offset brackets, 112 min). Another PSC
308 cell (Figure 5A, cyan arrowhead, 0 – 35min) extended long protrusions along the peripheral edge of the PSC
309 and was cleared by a macrophage (Figure 5A, yellow arrowhead, 42 – 49min). At imaging onset in the same
310 embryo, 2 PSC cells were laterally displaced (Figure 5B, arrowheads, 0 – 28min) but connected to the main PSC
311 collective by a thin protrusion (Figure 5B, green arrow, 0min). These 2 cells detached from the collective (7-
312 28min), underwent cell shape changes (elongated at 42-56min, brackets; highly protrusive at 77min), and
313 remained relatively stationary as the rest of the PSC and CBs migrated away (out of this focal plane).

314 Altogether, these data demonstrate that proper PSC formation requires 1) Slit signaling from the Vm and
315 dorsal vessel where signaling is necessary for proper alignment and organization of the dorsal vessel, which, in
316 turn, affects positioning of attached PSC cells; and 2) Robo activation in PSC cells for their persistent
317 association with one another as a collective (Figure 6).

318 **Discussion**

319 This is the first work to examine how the PSC is positioned. We describe the steady-state, coalesced
320 positioning of the cells comprising the PSC, characterize their migration, and reveal the signaling requirements
321 that facilitate their association and recruitment to the lymph gland. Altogether, the evidence we provide
322 culminates in a model in which the PSC migrates to the dorsal midline as a collective of cells—some adhere to
323 the dorsal vessel and the rest adhere to each other. We show that association of PSC cells requires input from
324 Vm and dorsal vessel, and we implicate Slit as a necessary signal. Though we have not ruled out direct Vm-to-
325 PSC signaling, we find at a minimum that Vm affects PSC positioning indirectly by its novel role in forming the
326 dorsal vessel. The intricate regulation described herein ensures that PSC cells achieve a precise steady-state
327 positioning as a coalesced group at the lymph gland posterior.

328 **Collective cell migration of the PSC**

329 Prior knowledge of the embryonic PSC has been focused on PSC cell specification (Crozatier et al., 2004;
330 Mandal et al., 2007). Thus, our live-imaging provides a substantial advancement by revealing PSC dynamics
331 after specification, during migration. PSC formation is an example of collective cell migration, reminiscent of
332 border cell migration in the *Drosophila* egg chamber and migration of the lateral line primordium in *Danio*
333 *rerio*. These cell collectives respond to guidance cues, and their constituent cells are highly protrusive and shift
334 position within the collective (Cliffe et al., 2017; Dalle Nogare et al., 2020; Haas & Gilmour, 2006; Peercy &
335 Starz-Gaiano, 2020). PSC migration is no different (Figure 1)– we observe extension and retraction of
336 protrusions on all surfaces of the collective except those in contact with CBs. This suggests that the migrating
337 PSC explores and responds to its environment. Some cells of the PSC maintain their position adjacent to the
338 dorsal vessel throughout the entirety of migration, while other cells exhibit fluidity within the collective. The
339 positional shifts suggest remodeling of adhesive contacts between cells—albeit in a coordinated manner to
340 achieve unidirectional migration for the entire cohort. Interestingly, circulating hemocytes can be seen
341 interacting with the PSC—hemocytes are known to deposit and remodel ECM (Bunt et al., 2010), which could
342 serve as a scaffold for adhesion molecules and as a substrate during migration. Indeed, we identified ECM
343 components surrounding the PSC and at its interface with the dorsal vessel. The characteristics noted above
344 could be further explored to improve our understanding not only of how the PSC is built, but more broadly of
345 collective cell migration.

346 **PSC heterogeneity**

347 For improved live-imaging we sought a PSC-specific marker but found most candidates to be expressed in only
348 subsets of PSC cells (unpublished data). The lack of homogenous expression across all cells suggests PSC
349 heterogeneity. The existence of fixed and fluid PSC cell positionings in the collective further hints at

heterogeneity—perhaps there are different types and polarities of adhesive molecules. If PSC heterogeneity exists at this early stage, its purpose is unknown. One possibility is that the fixed, dorsal vessel-adjacent PSC cells act as “leaders” while the more fluid PSC cells are “followers”, a common phenomenon in collective cell migration (Qin et al., 2021). The dorsal vessel has recently been shown to serve as a second hematopoietic niche component (Destalminil-Letourneau et al., 2021; Tian et al., 2023), so another possibility is that the fixed, dorsal vessel-adjacent PSC cells have a special function as intermediaries that coordinate communication between the niche components. That said, whether the niche components interact remains unknown. Finally, PSC heterogeneity in this early context could reflect a division of labor later, when the PSC regulates larval hematopoietic progenitors. Gene expression heterogeneity has been noted in the testis niche (Le Bras & Van Doren, 2006; Raz et al., 2023; Zheng et al., 2011), suggesting that this may be a conserved feature of niches which warrants further investigation. Our findings reported herein are foundational for future studies of PSC heterogeneity.

Coordinated input of extrinsic signals positions the PSC

We reveal that positioning the PSC requires input from different extrinsic sources. Organogenesis commonly relies on organ-extrinsic inputs. Like the PSC, the *Drosophila* excretory tubules require multiple inputs to navigate a complex signaling environment and achieve their final, precise positioning. To traverse the anterior-posterior axis, the tubules rely on alary muscles for posterior anchoring and on tissue sources located progressively more anteriorly for attractive BMP-dependent signaling (Weavers & Skaer, 2013). It is perhaps notable that the few well-studied examples of niche formation all involve extrinsic inputs. The mammalian intestine is organized into protrusive villi and invaginated crypts; Wnt and EphB3 signals emitted from the crypt base recruit niche cells from the crypt-villus interface to their final position in the compact troughs of the crypts (Batlle et al., 2002; Holmberg et al., 2006; van Es et al., 2005). The C. elegans gonadal niche cell relies on adjacent germ cell proliferation for propulsion towards its steady-state position at the apex of the gonad (Agarwal et al., 2022). A microniche of the mammalian hair follicle, the dermal papilla, originates via extrinsic Fgf20 signaling to dermal fibroblasts. The fibroblasts are recruited into a condensate via directed migration, and then the condensate is segregated deeper into the skin via epidermal invagination driven by reciprocal signaling between dermis and epidermis (Biggs et al., 2018). The *Drosophila* testis niche cells require FGF and Slit signals from Vm to migrate through the testis and assemble as a cap that is further compacted via actomyosin contractility (Anllo & DiNardo, 2022; Warder et al., 2024). Together with our findings on PSC formation, a paradigm for niche formation is emerging that, subsequent to niche cell specification, extrinsic input segregates niche cells from other constituents, and positions the collective toward one end of the tissue. Oftentimes positioning is accompanied by or precedes compaction of the recruited cells into a final niche shape/architecture.

We show that extrinsic Slit-Robo signaling is integral in establishing PSC position. Removing Slit causes PSC defects at the same frequency as removal of both canonical Robo receptors. This argues that in PSC formation, as in the gonadal niche and dorsal vessel, Slit only signals through Robo, and not through the non-canonical receptor, Dscam1 (Anllo & DiNardo, 2022; Qian et al., 2005). We noted that the PSC positioning phenotype was about 75% penetrant, and the severity of the defects varied. These observations argue that PSC formation relies on an additional cue(s) yet to be discovered. In fact, our lab showed in addition to Slit, gonadal niche formation requires the FGF ligand, *pyr*, and its receptor, *htl* (Anllo & DiNardo, 2022). Evidence for an additional PSC coalescence cue exists in later larval stages, as manipulated Insulin Receptor signaling was shown to disrupt PSC coalescence (Tokusumi et al., 2015). Unfortunately, most pathways are difficult to test for a role in PSC formation due to lack of an embryonic PSC-specific tool with the necessary temporal control.

Haploinsufficiency of Slit and Robo in PSC positioning

In the nervous system, one copy of the normal (WT) allele of Slit or Robo are typically sufficient for proper development (Kidd et al., 1999; Rothberg et al., 1988). In contrast, we find that about half of *robo2,robo1*

396 double heterozygotes or of *slit* heterozygotes have abnormal PSCs, suggesting haploinsufficiency in this
397 process. This observation for embryonic stages is supported by previous findings at later larval stages where
398 both *slit* or *robo2* heterozygotes have dispersed PSCs (Morin-Poulard et al., 2016). Perhaps haploinsufficiency
399 in the PSC reflects different regulation and function of the Slit-Robo pathway from the nerve cord.
400 Alternatively, because we identified that Slit-Robo signaling is required within both CBs and PSC for proper
401 development of both tissues, the haploinsufficiency may reflect a combinatorial defect caused by diminished
402 signaling in both tissues. Furthermore, we are surprised that *robo2* and *robo1* single mutants have a similar
403 frequency of abnormal PSCs because in the embryo Robo1 is expressed in all PSC cells whereas Robo2 appears
404 to be expressed in only one PSC cell. However, it is possible that all PSC cells express Robo2 and our finding
405 reflects limited detection ability with the Robo2-GFP reporter. An alternative, intriguing possibility is that the
406 Robo2-expressing PSC cell is the "leader" in PSC migration, and without Robo2 signaling in the leader, the
407 collective fails to migrate appropriately, or the followers fail to remain properly adherent.

408 Morin-Poulard et. al. show that all larval PSC cells express Robo2, and it has a more prominent role than Robo1
409 in maintaining PSC coalescence (termed 'clustering' in their work) during larval stages (Morin-Poulard et al.,
410 2016). In fact, they found Robo1 knockdown alone was insufficient to disrupt clustering. Taken together with
411 our work, perhaps this indicates that Robo1 is more important for first establishing PSC coalescence and Robo2
412 is more important for maintaining it. Most manipulations occurred after the PSC had already formed, and
413 therefore the changes reported cannot stem from defects during establishment but rather from dispersion of
414 the cluster after it formed. One experiment without temperature control that could have diminished Robo
415 signaling in PSC and CBs early (Antp>Robo RNAi), at about the time of PSC specification, generated a more
416 dispersed late larval PSC compared to Robo knockdown subsequent to PSC formation. One can imagine that
417 aberrant embryonic PSC positioning would become exacerbated and increasingly catastrophic as the PSC and
418 nearby progenitors proliferate throughout larval stages. The fact that earlier Robo knockdown worsened the
419 larval PSC defect supports our finding that Slit-Robo signaling is vital to establish PSC coalescence.

420 **Function of Slit-Robo in PSC positioning**

421 Determining how Slit affects a given process is complex because it can act as an attractive or repulsive cue, or
422 even affect cell adhesion, and in some instances the outcome relies on whether Slit is cleaved by Tok (Englund
423 et al., 2002; Kellermeyer et al., 2020; Kolesnikov & Beckendorf, 2005; Kramer et al., 2001). Thus, elucidating
424 the role of the Slit-Robo pathway in PSC formation is difficult. Upon compromising the pathway, we observed
425 PSC mis-positioning in all directions. Also, we found that Slit is required in both Vm and dorsal vessel, and the
426 role for each tissue in PSC formation is intertwined. The existence and relative positioning of two Slit sources,
427 the reliance on one for positioning of the other, and the inconsistent direction of PSC mis-positioning suggest
428 that it is too simplistic to ask whether Slit is acting as a repulsive or attractive cue for PSC cells. Notably, mis-
429 positioned PSC cells adopted aberrant contacts with CBs, LG, and pericardial cells of the dorsal vessel. When
430 reported in the dorsal vessel, this inappropriate mixing of cells was attributed to improper polarity of cell
431 adhesion molecules (Medioni et al., 2008b; Qian et al., 2005; Santiago-Martínez et al., 2006). Furthermore, Slit
432 has been shown to be important for maintaining adhesion amongst larval PSC cells (Morin-Poulard et al.,
433 2016). Taken together with our data, we reason that during PSC migration Slit must affect the ability of PSC
434 cells to properly adhere to the dorsal vessel and to one another. In this manner, Slit facilitates PSC cell
435 association as a compact cluster.

436 The various effects we have documented for Slit signaling indicate that downstream regulation is likely
437 complex and dependent on the specific context, in time and space. Morin-Poulard et. al. show that the Slit-
438 Robo pathway maintains clustering of larval PSC cells via DE-Cadherin and Cdc42 (Morin-Poulard et al., 2016);
439 however, our data indicate different effectors are at play during PSC formation, as we detect no DE-Cad in the
440 embryonic PSC (data not shown). Additionally, whereas constitutively active Cdc42 in the larval PSC caused
441 dispersion(Morin-Poulard et al., 2016), our attempt to elicit PSC dispersion with this manipulation in the

embryo yielded normally coalesced PSCs (data not shown). Therefore, we reason that different downstream effectors are engaged by the Slit-Robo pathway for initial positioning of the PSC.

This study was limited by the lack of a truly PSC-specific driver—a tool that would improve live-imaging and allow testing of potential Slit-Robo pathway effectors. We and others observe Fasciclin III, a homotypic cell adhesion molecule, in the PSC (unpublished data and Mandal et al., 2007), however, it is first detectable too late in embryogenesis to function during PSC formation. Thus, the particular adhesion molecules that maintain association of PSC cells as they migrate remain unknown. Elucidating this tool will facilitate interrogation of how Slit-Robo signaling impacts PSC adhesion to the dorsal vessel and amongst itself.

Passive and active roles for Slit-Robo signaling in PSC positioning

Due to the necessity of autocrine Slit-Robo signaling in dorsal vessel formation (MacMullin & Jacobs, 2006b; Medioni et al., 2008a; Qian et al., 2005; Santiago-Martínez et al., 2006, 2008), it was challenging to distinguish whether effects on the PSC were secondary to mis-positioned CBs, or primary consequences of diminished Robo activation in PSC cells. Our analysis of *robo2,robo1* double mutants along with the registration marker, svp-lacZ, strongly suggests both passive mis-positioning of PSC cells via attachment to mis-positioned CBs and a requirement for Robo activation directly in PSC cells. A direct requirement for Robo in PSC cells is further suggested in *slit* mutant live-imaging. Here, the lateral-most PSC cells separated from the main cluster even though no CBs were nearby (Figure 5B). Perhaps during normal migration these more 'fluid', lateral PSC cells possess a stronger requirement for Robo activation and require direct input to achieve that. In this view, those PSC cells that are passively mis-positioned in mutants are the same PSC cells that remain affixed to the dorsal vessel during normal migration. Alternatively, or additionally, passive mis-positioning of CB-adjacent PSC cells might occur due to improper polarization of adhesive molecules, whereas separation of lateral PSC cells from the collective might occur due to a total loss of adhesive molecules.

Identification of novel mechanisms controlling dorsal vessel development

Our investigation of PSC formation unexpectedly revealed new insights about the dorsal vessel. We uncover a novel role for Vm in positioning the dorsal vessel. In Vm manipulations we noted abnormal positioning of Antp+ CBs, and upon further investigation of mutants lacking Vm, we show that large portions of the dorsal vessel are malformed. The twisting phenotype we observe suggests luminal collapse, and, thus, Vm may contribute to lumen formation. Alternatively, Vm could affect CBs at the time of their specification. Both Vm and CBs originate from dorsal mesoderm, and we learned that Vm is able to act at this early timepoint via our finding that early Vm signals influence PSC positioning. Additionally, we were surprised in dorsal vessel ablation experiments to observe more apparent ablation in mid-stage embryos than late-stage. Note that the CBs should be post-mitotic (Gajewski et al., 2000; Han & Bodmer, 2003; Ward & Skeath, 2000). Thus, under challenge conditions CBs fill the gaps by either re-entering the cell cycle to produce new daughters, or, more likely, by elongating to fill gaps. Regardless of mechanism, this observation suggests plasticity of the dorsal vessel upon challenge.

Connecting niche structure, position, and function

The coalesced nature and posterior positioning of the PSC are its most prominent features. The consistency of these features suggested that they are under tight regulation, as we report here, and strongly indicates their relevance to function of the PSC. Though we have yet linked the precise architecture of the embryonic PSC to function, the specific architectures of multiple other niches have been shown to be functionally relevant. In the *Drosophila* gonad, a coalesced and compact niche is necessary for proper germline stem cell maintenance, niche signaling, and for orienting characteristically orthogonal germline stem cell divisions (Anllo & DiNardo, 2022; Warder et al., 2024). In the mammalian hair follicle, niche position determines stem cell fate (Rompolas et al., 2013). *Drosophila* neural stem cells are supported by glia, and the precise morphology of this encasing niche is required for newborn neuronal survival, and therefore homeostasis of the entire nerve cord (Spéder &

Brand, 2018). Most pertinently, recent work has shown that the larval PSC communicates amongst itself via a calcium signaling network. The integrity of this network is gap junction-dependent and is required for the PSC to emit proper levels of a progenitor maintenance signal (Ho et al., 2021, 2023). We find it reasonable to postulate that a dispersed PSC would exhibit defective calcium signaling such that the PSC would lack coordinated maintenance of progenitors, thereby leading to an imbalance in the ratio of progenitors to differentiated hemocytes in the gland. Future experiments will determine how PSC coalescence is functionally relevant to its regulation of hematopoietic progenitors.

Figure Legends

Figure 1. Live-imaging reveals dynamics of PSC migration and presence of nearby muscles.

All images are oriented with anterior to the left and posterior to the right. A) Schematic depicts prior knowledge of PSC migration. Prospective cells of lymph glands (hematopoietic progenitors, magenta, and PSC, green) and cardioblasts (blue) of the dorsal vessel are specified as distinct clusters prior to migration onset around stage 13 (left). Around stage 16 (right) lymph gland clusters have coalesced and flank the dorsal vessel at the dorsal midline; bilaterally symmetric counterparts are aligned. B-F) Fixed w^{1118} embryos stained for Antp and Odd to label the PSC. B) Stage 14 PSC (green) is lateral in embryo, tightly clustered, and flanks 2 Antp+ CBs (blue). C) Late stage 14 PSC is more dorsal, flanking 2 Antp+ CBs. D) The stage 15 PSC is even more dorsal, elongated, and flanks 4 Antp+ CBs; contralateral Antp+ CBs in view. E) Late stage 15 PSC is more medial and compact. F) Stage 16 LGs and CBs at final position at dorsal midline, right LG partially in view. PSC is compact and coalesced at LG posterior, flanking Antp+ CBs. Antp+ CBs (yellow brackets) are neatly aligned in stereotypical 2x4 organization. B'-F') Schematics depicting relevant cell types in B-F: hematopoietic progenitors (magenta), PSC (green), and Antp+ cardioblasts (blue). G-J) Live-imaging stills from Hand-RFP,Antp-GAL4,10xUAS-myr:GFP embryos; RFP in magenta and GFP in white. G) Timelapse shows dorsolateral view of PSC (magenta and white cells above green underline and below string of CBs, arrows) migrating as a collective from migration onset (0m), when the PSC is lateral, to migration completion (around 2h50m), when the PSC is dorsal. Arrowhead indicates fixed positioning of the posterior-most PSC cell in the collective. H-H''') Live-imaging stills show PSC protrusions during mid-migration. H) Merge shows positional relation of PSC (white and magenta) and its protrusions to rest of lymph gland and CBs (along top of image). H'-H''') Only GFP channel. Progressively shallower z-slices of same PSC. H') Anterior protrusions; some short (arrowheads) and one long (bracket) that encases lymph gland. H'') Posterior protrusion (bracket). H''') Green dot indicates dorsal-most PSC cell with short, branching protrusions (arrowheads). Much of image contains Antp+ epidermis. I) Live-imaging stills of GFP channel only show PSC cells shifting position within collective. Initially connected yellow and cyan PSC cells (0m, arrowhead) become separated by intercalation of magenta and green PSC cells while the posterior-most, dorsal vessel-adjacent PSC cell (orange dot) remains at a fixed position in the collective. J) Same embryo as (G), GFP channel only. For the entire timelapse PSC cells migrate dorsally in close association with concurrently migrating neighbor tissues, CBs and Vm. Posterior-most PSC cell (arrowhead) maintains its dorsal vessel-adjacent position throughout. 0m inset shows PSC proximity to Vm and 2h50m inset shows PSC proximity to CBs. J') Schematics depict relevant cell types for each panel of J time series: cardioblasts (blue), PSC (green), and visceral mesoderm (orange). K) Live-imaging series from dorsal vantage point shows A1 AMs (magenta; labeled with *org-1*-HN39::RFP) contact PSCs (green outlines; labeled by Antp>CD8::GFP) throughout the timelapse as both tissues migrate to dorsal midline. L) Schematics depict the relative positioning of the tissues identified to be near the PSC at migration onset (left) and completion (right).

Figure 2. Visceral mesoderm and cardioblasts are required for PSC formation.

All PSCs, co-labeled by Antp and Odd, are viewed dorsally from st16 or 17 embryos unless otherwise noted. A and B) LGs with normally-positioned PSCs outlined in yellow from control (A) and AM-ablated (B) embryos with AMs labeled by AME-Gal4 driven mCD8:GFP. A' and B') GFP channel only with PSC outlines overlayed. C) PSC positioning quantification. D and E) *bin* heterozygotes labeled with Fas3, lateral views. D) green bracket indicates st12 Vm. E) st16 with green arrow indicating first Vm constriction that segregates two sections of gut. F) *bin* heterozygote LGs with normal PSC positioning. G and H) lateral views of *bin* mutants with minimal (G, st12) and absent (H, st16) Vm. I) *bin* mutant LGs with dispersed PSCs (cyan arrowheads). J) PSC positioning quantification including analysis of bin^{R22}/bin^{S4} transheterozygous mutants. K-P) control embryos (K-M) compared to Vm-ablated embryos (N-P). K) Lateral view of normal st11 Vm labeled by Fas3. Founder cells are below magenta line and fusion competent myoblasts are between magenta and green lines. L) Dorsal view of normal st16 Vm. M) Normal PSC positioning, yellow outlines, in control. N) Fusion competent myoblasts

absent, green brackets, in st11 Vm ablated embryo. Most founder cells present with occasional gaps. O) Vm absent in st16 Vm ablated embryo. P) Abnormal PSC positioning, cyan arrowheads. Q) PSC positioning quantification. R and S) st15 LGs with cardioblasts labeled by Mef2 in control (R) and CB-ablated embryos (S). R) Normal PSC positioning, yellow outlines. S) CBs ablated on left side, bracket, and corresponding PSC is mis-positioned, arrowheads, while right side CBs are intact and the R PSC is positioned normally, yellow outline. R' and S') Mef2 channel only. T) Quantification comparing PSC positioning in control embryos to positioning of PSCs with ablated ipsilateral CBs. Scale bars as indicated. Ns = not significant, *p<0.05, **p<0.01, ***p<0.001, ****p<0.0001, Fisher's Exact test. Sample sizes as indicated.

Figure 3. Slit from Vm and CBs signals through Robo for PSC positioning.

All PSCs, co-labeled by Antp and Odd, are viewed dorsally from st16 or 17 embryos. Normally coalesced and positioned PSC cells are outlined in yellow; dispersed PSC cells indicated by cyan arrowheads A) Schematic of dorsal st14 embryo. Relevant tissues are indicated; Vm is ventral to the rest. B) Slit expression in st14 CBs, blue outline, and Vm, orange outline; these tissues are in reversed orientation from the schematic due to embryo tilt, and the projection necessary to have both tissues in view. C-E) Analysis of PSC positioning in *sli*^{2} heterozygotes (C, normal PSCs) and *sli*^{2} mutants (D, dispersed PSCs), with frequency of positioning phenotype quantified in E. F-L) Analysis of PSC positioning under various *robo* depletion scenarios. *robo1* heterozygote (F) and *robo2* heterozygote (G) with normal PSCs. H) *robo1,robo2* double heterozygote with abnormal PSCs. *robo1* single (I), *robo2* single (J), and *robo1, robo2* double (K) mutants with abnormal PSCs; frequency of positioning phenotype quantified in L ('H' is heterozygote, 'M' is mutant). M-U) Analysis of PSC positioning when Slit signaling from CBs is compromised; frequency of PSC positioning phenotype quantified in U. M, O, Q, S) Slit expression in Mef2 labeled cardioblasts of controls (M) and tinCΔ4-GAL4 driven Slit RNAi knockdown (O and Q) or Robo1 overexpression (S) embryos. M', O', Q', S') Slit channel only. N) Control with normal PSCs. P, R, T) Dispersed PSCs upon compromised Slit signaling from CBs. V-BB) Analysis of PSC positioning when Slit signaling from Vm is compromised; frequency of PSC positioning phenotype quantified in BB. V and Y) Schematics of dorsolateral st14 control (V) or bap-GAL4 driven Robo1 overexpression (Y) embryos with relevant tissues and proteins indicated. W) Diffuse Slit expression in Fas3-labeled Vm of st14 control embryo. Z) Slit trapping at Fas3-labeled Vm membranes in bap-GAL4 driven Robo1 overexpression embryo. W' and Z') Slit channel only. X) Normally positioned PSCs and Antp+ CBs (brackets) in control. AA) Abnormally positioned PSC and Antp+ CBs (brackets) in bap-GAL4 driven Robo1 overexpression embryo. Scale bars as indicated. Ns = not significant, *p<0.05, **p<0.01, ***p<0.001, ****p<0.0001, Fisher's Exact test. Sample sizes as indicated.

Figure 4. PSC positioning requires Vm-mediated dorsal vessel organization and Robo activation in PSC cells.

A-C) Analysis of dorsal vessels with and without Vm; phenotype frequencies quantified in (C). A and B) Mef2-labeled CBs and Slit-labeled lumens of dorsal vessels. A) dorsal vessel of sibling control, captured in 4.0µm projection, shows normal, neatly-aligned CB organization. B) *bin*^{R22} mutant with twisted dorsal vessel (bracket), fully captured only by projection of an 8.0µm deep stack. B') twisted phenotype evidenced by the absence of the sunken portion in the first 3.5µm;. B'') 3.5-8µm projection. D) Schematics depicting three expectations for PSC and CB positioning. In controls (left), PSCs are coalesced and adjacent to CBs. In *robo2*,*robo1* mutants, either PSC cells are associated with mis-positioned CBs (middle), suggesting passive displacement of the PSCs; *or* displaced PSC cells are sometimes separate from mis-positioned CBs (right), suggesting the PSC cells themselves require activated Robo signaling. E-I) Analysis of CB and PSC positioning with additional CB marker, *svp*-LacZ. Brackets indicate normally-positioned CBs. Yellow outlines indicate normally-positioned PSC cells. Arrowheads indicate abnormally-positioned PSC cells; green arrowheads indicate passive mis-positioning and magenta arrowheads are displaced PSC cells without a similarly displaced CB nearby. Arrows indicate the next set of svp+ CBs to the posterior. E) Control with normally-positioned PSCs and CBs; second set of svp+ CBs (arrow) nearby. F) *robo2*,*robo1* mutant with abnormal CB positioning; Antp+ CBs are dispersed and the second set of svp+ CBs (arrow) are displaced far posteriorly. PSCs display both passive mis-positioning posteriorly

587 (green arrowheads) and mis-positioning without a similarly mispositioned CB nearby (magenta arrowheads;
588 bottom PSC cell invaded midline and top PSC cell is displaced laterally). G) *robo2*,*robo1* mutant with left side
589 CBs positioned normally (brackets) and the second set of svp+ CBs in view (arrow); despite normal CB
590 positioning, the ipsilateral PSC has a mis-positioned cell (magenta arrowhead). Right side CBs positioned
591 abnormally (an Antp+ CB is displaced laterally and the second set of svp+ CBs are displaced posteriorly, not in
592 view); correspondingly, the ipsilateral PSC has two laterally displaced cells (green arrowheads). H) Frequency of
593 mis-positioning of both a PSC and the ipsilateral CBs; this occurs more frequently in *robo2*,*robo1* mutants than
594 heterozygotes. I) Frequency of correlated mis-positioning of PSCs and CBs. Both *robo2*,*robo1* heterozygotes
595 and mutants have CB-independent instances of PSC mis-positioning. Sample sizes as indicated. **p<0.01,
596 ****p<0.0001, Fisher's Exact test. Scale bars as indicated.

597 **Figure 5. During migration Slit is required for proper PSC adhesions to CBs and for association of the PSC**
598 **collective.**

599 A and B) timelapse imaging of *sli* mutant embryo with LG and PSC labeled by Hand-RFP, Antp>myrGFP;
600 dorsolateral view. A) The line of GFP+ cells within the brackets are Antp+ CBs; GFP+ cells below this are Antp+
601 PSC cells. Elongated PSC cell (cyan arrowhead; 0-35') cleared by macrophage (yellow arrowhead; 42-49').
602 Anterior and posterior edges of another PSC cell (cyan dot) bridges separated CBs (0-70'); same PSC cell
603 aberrantly contacts a contralateral Antp+ CB (yellow dot; 49-70'). Persisting gap in CBs (arrows; 112') evident in
604 same region. A') just GFP channel. Brackets indicate mis-aligned contralateral Antp+ CBs. B) Cells within the
605 yellow brackets are Antp+ CBs. Same PSC as (A) contains two laterally displaced PSC cells (cyan arrowheads; 0-
606 28') barely attached (green arrow; 0') to main cluster. These cells are disconnected from the main cluster (7')
607 and remain stationary as the other PSC cells and CBs migrate away (7-77'). The disconnected PSC cell(s) change
608 shape (cyan brackets) and develop membranous spikes (77' arrowhead). Scale bars as indicated.

609 **Figure 6. Model of PSC formation.**

610 **Figure S1. ECM components surround the PSC and AM encases PSC cells.**

611 A and B) ECM components Perlecan and Viking (Collagen IV subunit) surround migrating PSCs. A) *perlecan*-GFP
612 reporter, white, surrounds migrating Antp-labeled PSC cells, cyan arrowheads, of st14 embryo. B) *viking*-GFP
613 reporter, white, surrounds migrating PSC collective on embryo left side, cyan outline, and a single PSC cell on
614 the right side, arrowhead. A' and B') GFP channel only. C-E) *org-1*-RFP embryos with PSCs labeled by Antp,
615 yellow brackets or arrowheads. C) Alary muscle of first abdominal segment (A1 AM), cyan, contacts posterior
616 of PSC collective in st15 embryo. D) A1 AMs contact entire PSC collectives of st17 embryo. E) st16 embryo with
617 individual A1 AM fibers encasing two PSC cells, arrowheads. E') RFP channel alone. Scale bars as indicated.

618 **Figure S2.**

619 All PSC positioning analyses were completed on st16 or st17 embryos by co-labeling with Antp and Odd. A)
620 Quantitation of PSC cells in controls and AM-ablated embryos. Not significant (ns), Mann-Whitney test. B)
621 lateral view of st13 embryo stained for Antp (white) and Bin (red). Antp labels PSC collective (arrowhead) and
622 Bin is expressed in Vm (brackets), as expected. B') Magnified view of Antp+ collective (outline) shows no
623 detectable Bin. B'') Bin channel only; PSC collective outlined. C and D) Fas3-labeled Vm (white) of st11 control
624 (C) and FCM-ablated (D) embryos also stained for Bin (red). E) Bin expression is reduced in remaining FCs of
625 Vm-ablated embryos. ****p<0.0001, Mann-Whiteny test. F-K) Analysis of *bap*^{208} sibling controls (F-H) and
626 hypomorphic mutants (I-K). F and I) lateral view of st11 Fas3-labeled Vm precursors of control (F) and mutant
627 (I), which has almost normal Vm organization with occasional gaps. G) dorsolateral view of Fas3 stained st16
628 sibling control embryo with normal Vm morphology. H) Sibling control LGs with normal PSCs. J) Dorsolateral
629 view of Fas3 stained late stage mutant embryo with disorganized Vm that is missing in the midline region
630 where the PSC is normally located. K) *bap*^{208} mutant LGs with normal PSCs. L) Quantification of frequency of
631 PSC positioning phenotype in *bap*^{208} sibling controls and mutants; ns, Fisher's Exact test. M-Q) analysis of PSC

632 positioning for various *jeb* alleles; frequency of phenotypes quantified in Q (ns, Fisher's Exact test). M and N)
633 LGs with normal PSC positioning from *jeb*^{weli} heterozygous (M) and homozygous (N) mutant. O and P) LG with
634 normal PSC positioning from a sibling control (O) and a *jeb*^{weli}/*jeb* Df transheterozygous mutant (P). Scale bars
635 as indicated. Sample sizes as indicated.

636 **Figure S3. Robo1 and Robo2 are expressed by PSC cells.**

637 A) Robo1 expression (cyan) on PSC cell membranes (arrowheads) of st14 embryo stained for Antp; brackets are
638 two of the eventual 4 Antp+ CBs. A') Robo1 channel alone. B) *robo2*-GFP reporter expression (cyan) on
639 membrane of single PSC cell (arrowhead) of st15 embryo stained for Antp; brackets enclose Antp+ CBs. B') GFP
640 channel alone.

641

642

643

Acknowledgements:

We thank the Bloomington Drosophila Stock Center (NIH P40OD018537), J. Skeath, J. Reinitz, E. Furlong, G. Bashaw, M. Crozatier, U. Banerjee, M. Frasch, G. Vogler, and DSHB for antibodies and stocks. We thank CDB microscopy core director Andrea Stout for advice on imaging. Thanks to B. Warder, G. Vida, G. Bashaw, and the K. Lenhart lab for input during this project. This work was supported by NIH grants T32 HD083185 and F31 HD111208 to KAN; R01 GM138705 to KFL; F32 GM125123 to LA; R35 GM136270 and R03 HD111973 to SD.

Materials and Methods

In this study we used FlyBase (releases 2020_06 - 2024_02; Jenkins et al., 2022) to find information on phenotypes, function, stocks, and gene expression. All data describe biological replicates. Each experiment was repeated at least once. The Mann-Whitney test was used for statistical comparison of two groups of unpaired numerical data with non-Gaussian distribution. Fisher's exact test was used for statistical comparison of two groups of categorical data. All corresponding data spreadsheets depicted by the graphs herein are available upon email request.

Drosophila genetics:

Detailed information on the *Drosophila* strains used in this study is in the Key Resources Table. Controls were GAL4 only, a cross to w^{1118}, or a sibling control identified by a fluorescent balancer. This study generated the following embryo genotypes by combination into a stock (available upon email request) or obtained through a cross:

Hand-RFP,Antp-GAL4,UAS-myr:GFP
UAS-CD8:GFP / org-1-HN39-RFP ; Antp-GAL4 / +
UAS-CD8:GFP / + ; tupAME-GAL4 / +
UAS-CD8:GFP / UAS-grim ; tupAME-GAL4 / TM6Hu or MKRS
bin^{R22} / +
bin^{R22} / bin^{S4}
bap-GAL4 ; + / CyODfd-YFP ; bap-GAL4
bap-GAL4 ; + / UAS-hid ; bap-GAL4
UAS-grim ; tinCΔ4-GAL4
$robo1^{GA285}$ / +
$robo2^{1}$ / +
$robo1^{GA285}$,$robo2^{123}$ / +
tinCΔ4-GAL4 / +
UAS-sli RNAi / + ; tinCΔ4-GAL4 / UAS-dcr-2
UAS-dcr-2 / + ; tinCΔ4-GAL4 / UAS-sli RNAi
UAS-Robo1 OX / + ; tinCΔ4-GAL4 / +
bap-GAL4 ; + / UAS-Robo1 OX ; bap-GAL4 / +
$robo1^{GA285}$,$robo2^{123}$ / CyO,hindgut-LacZ ; *svp*–LacZ / TM6Dfd-GFP
sli^{2} ; Hand-RFP,Antp-GAL4,UAS-myr:GFP
jeb^{weli} / +
jeb^{weli} / *jeb*[Df]

Embryo collection:

Unless otherwise noted, embryos were collected on apple juice agar plates overnight at 25 degrees, unless an experiment involved a Gal4, in which case collections occurred at 29 degrees. The next morning embryos were dechorionated in 50% bleach.

Embryo fixation:

Using a paintbrush, embryos were transferred from a collection basket to a 50/50 mixture by volume of heptane and 4% paraformaldehyde in Buffer B (16.7mM KPO_4, pH 6.8; 75mM KCl; 25mM NaCl; 3.3mM $MgCl_2$)(de Cuevas & Spradling, 1998). Embryos were fixed on a rocker for 15 minutes, then fixative was removed. An equal volume of MeOH was added and the vial was shaken vigorously for about 5 seconds to remove vitelline membranes. The heptane and MeOH mixture was discarded, and the embryos were rinsed three times with MeOH.

697 **Embryo staging and genotyping:**

698 Embryos were staged according to Atlas of *Drosophila* Development (Hartenstein, 1993). Embryos were
699 genotyped according to presence of a balancer chromosome: CyO, P{Dfd-EYFP}); or CyO,P({Wg-lacZ}); or CyO,
700 hindgut-lacZ; or TM6, P{Dfd-EYFP}, Sb, Hu, e.

701 **Immunostaining:**

702 Manipulations were room temperature unless otherwise noted. Embryos were rehydrated in 50%MeOH/50%
703 PBS (10mM Na_2 HPO_4; 1.8mM KH_2PO_4; 2.7mM KCl; 137mM NaCl; pH 7.4), followed by 100% PBS. Embryos
704 rocked for 5 minutes in PBS with 0.1% Triton X-100 (PBST), then 1 hour in 4% normal donkey serum in PBST.
705 Embryos were then transferred to a rocker at 4 degrees until the end of the day or began incubation in primary
706 antibody solution. The next day embryos were rinsed 3 times in PBST then rocked in PBST for 1 hour, incubated
707 in secondary antibody solution for 1 hour, rinsed 3 times in PBST, rocked in PBST for 1 hour, equilibrated in 50%
708 glycerol/50% Ringer's solution (5mM HEPES, pH 7.3; 130mM NaCl; 5mM KCl; 2mM $MgCl_2$; 2mM $CaCl_2$) for 15
709 minutes or overnight at 4 degrees, then mounted in 2% nPropyl-gallate in 90% glycerol. Primary antibodies
710 were diluted in normal donkey serum as follows: mouse antibody against Antp (1:50; DSHB, 8C11), rabbit
711 antibody against Odd skipped (1:400; gift from James Skeath, Washington University School of Medicine) chick
712 antibody against GFP (1:1500; Aves Labs, GFP-1020), rabbit antibody against RFP (1:1000; Abcam, ab62341),
713 mouse antibody against Fasciclin 3 (1:50; DSHB, 7G10), rabbit antibody against Mef2 (1:1000; DSHB), guinea
714 pig antibody against Odd skipped (1:1200; gift from John Reinitz, University of Chicago), rabbit antibody against
715 Bin (1:100; gift from Eileen Furlong, EMBL), mouse antibody against Slit (1:200; gift from Greg Bashaw,
716 University of Pennsylvania), mouse antibody against Robo1 (1:200; gift from Greg Bashaw, University of
717 Pennsylvania), chick antibody against LacZ (1:1000; Abcam, ab9361-250). Secondary antibodies (Alexa Fluor
718 488, Cy3, Cy5, and Alexa Fluor 647; Molecular Probes or Jackson ImmunoResearch) were all used at
719 3.75ug/mL, for 1 hour.

720 **Live-imaging:**

721 After dechorionation, embryos were selected by stage and transgene expression, using a stereoflouorescent
722 microscope, transferred to a piece of agar, and then oriented in a line with the ventral/ventrolateral surface
723 facing up – hanging off the edge of the agar. A heptane-glue mixture was dried as a strip on a glass slide, and
724 that surface touched to the embryos for transfer (now dorsal/dorsolateral surface of embryos faces up). 3uL of
725 halocarbon oil was added atop the embryos. Bridging coverslips were glued to the slide on either side of the
726 line of embryos, then the main coverslip was laid atop the bridging coverslips. We imaged every 5-10 minutes
727 for 2-4.5 hours; Z-stacks spanned 25-40uM with 0.3-1.0uM step sizes.

728 **Microscopy:**

729 Fixed embryos were imaged on a Zeiss Axio Imager with ApoTome using a 40x, 1.2 NA water immersion
730 objective or a 20x, 0.8 NA objective; z-steps were 0.5 – 1.0uM. All live-imaging except for alary muscle imaging
731 occurred with a CrestOptics X-Light V3 spinning disk confocal microscope using a 60x, 1.3NA silicone
732 immersion objective; images were captured with two pco.edge 4.2 bi sCMOS cameras operated by VisiView
733 (Visitron) software. Alary muscles were live-imaged with an IX7 Olympus spinning disk confocal using a 63x, NA
734 1.2 water immersion objective and captured with an EMCCD camera (Hamamatsu photonics, model C9100-13)
735 controlled by MetaMorph software.

736 **PSC positioning phenotypic characterization:**

737 We used immunostains for the accepted markers, Antp and Odd, to identify PSC cells. Sometimes images
738 contained Antp+ and Odd+ cells in epidermal stripes anterior to the LG; these were not considered PSC cells.
739 An embryo was scored as having 'normal' PSC positioning if both PSCs were 1) coalesced within one nuclear
740 diameter of one another, 2) adjacent to the dorsal vessel, and 3) at the same dorsal-ventral position as the

741 posterior-most cells of the lymph gland. Abnormal PSC positioning presented as a range of phenotypes
742 including PSCs dispersed into multiple groups, and PSCs that were coalesced but not located at the LG
743 posterior. Fisher's Exact test was used for statistical analysis and $p < 0.05$ was considered statistically
744 significant.

745 **AM ablation PSC cell counting:**

746 We considered a cell to be a PSC cell if it was co-labeled by Antp and Odd and was not located in epidermis.
747 Number of PSC cells was recorded separately for the left and right PSCs of each embryo, and the total number
748 of PSC cells per embryo was plotted. The Mann-Whitney test was used to determine a non-significant
749 difference with $p > 0.05$.

750 **Bin fluorescent intensity:**

751 For 9 sibling controls and 10 Vm-ablated embryos, a normalized Bin fluorescent intensity was calculated for 3
752 different regions of st11 Vm founder cells with Bin-stained nuclei and Fas3-stained membranes. For st11
753 embryos imaged laterally, Fas3 labels the 2 lateral surfaces of a given Vm founder cell membrane. ImageJ
754 software was used to extract fluorescent intensity values for regions of interest including large non-positive
755 background regions in the embryo, founder cell nuclei, and founder cell membranes. Bin intensity for a given
756 region was calculated by normalizing the background subtracted Bin level of a single representative nucleus to
757 the average background subtracted Fas3 level of at least the 2 lateral surfaces of that same cell; most often an
758 average Fas3 level for a given region was calculated based on the membranes of 2-4 founder cells. The
759 normalized Bin fluorescent intensity for a given region is plotted. The Mann-Whitney test was used for
760 statistical analysis to determine a significant difference of $p < 0.05$.

761 **Tissue ablations:**

762 <u>AM ablation:</u> the tupAME-GAL4 driver was combined with UAS-CD8:GFP for AM visualization, and GFP-labeled
763 AMs were clearly visible in st13 controls. This line was crossed to UAS-grim to generate AM-ablated embryos;
764 AMs were ablated by st14.

765 <u>CB ablation:</u> flies with the tinCΔ4-GAL4 driver were crossed to flies with either UAS-grim or UAS-hid and
766 embryos were collected overnight at 29 degrees. Expression of either pro-apoptotic gene led to quite effective
767 dorsal vessel ablation, but there were also defects in either Vm (for Grim) or in germband retraction (for Hid;
768 data not shown), which could confound a PSC positioning analysis. We circumvented this issue by lowering
769 GAL4 activity—embryos from the cross to UAS-grim were collected at 25 degrees—which yielded relatively
770 normal Vm but successfully ablated CBs beginning at st14.

771 **Slit RNAi in dorsal vessel:**

772 Two independent UAS-controlled RNAi's targeting different regions of Exon 4 of Slit along with UAS-controlled
773 Dcr2 were driven by tinCΔ4-GAL4. Knockdown was evident at st14, the same stage when Slit expression
774 becomes discernable in control CBs.

775

References

Agarwal, P., Shemesh, T., & Zaidel-Bar, R. (2022). Directed cell invasion and asymmetric adhesion drive tissue elongation and turning in C. elegans gonad morphogenesis. *Developmental Cell*, *57*(17), 2111-2126.e6. https://doi.org/10.1016/j.devcel.2022.08.003

Anllo, L., & DiNardo, S. (2022). Visceral mesoderm signaling regulates assembly position and function of the Drosophila testis niche. *Developmental Cell*, *57*(8), 1009-1023.e5. https://doi.org/10.1016/j.devcel.2022.03.009

Anllo, L., Plasschaert, L. W., Sui, J., & DiNardo, S. (2019). Live imaging reveals hub cell assembly and compaction dynamics during morphogenesis of the Drosophila testis niche. *Developmental Biology*, *446*(1), 102–118. https://doi.org/10.1016/j.ydbio.2018.12.014

Baldeosingh, R., Gao, H., Wu, X., & Fossett, N. (2018). Hedgehog signaling from the Posterior Signaling Center maintains U-shaped expression and a prohemocyte population in Drosophila. *Developmental Biology*, *441*(1), 132–145. https://doi.org/10.1016/j.ydbio.2018.06.020

Banerjee, U., Girard, J. R., Goins, L. M., & Spratford, C. M. (2019). Drosophila as a genetic model for hematopoiesis. *Genetics*, *211*(2), 367–417. https://doi.org/10.1534/genetics.118.300223

Batlle, E., Henderson, J. T., Beghtel, H., van den Born, M. M. W., Sancho, E., Huls, G., Meeldijk, J., Robertson, J., van de Wetering, M., Pawson, T., & Clevers, H. (2002). β-Catenin and TCF Mediate Cell Positioning in the Intestinal Epithelium by Controlling the Expression of EphB/EphrinB. *Cell*, *111*(2), 251–263. https://doi.org/10.1016/S0092-8674(02)01015-2

Biggs, L. C., Mäkelä, O. J. M., Myllymäki, S. M., Das Roy, R., Närhi, K., Pispa, J., Mustonen, T., & Mikkola, M. L. (2018). Hair follicle dermal condensation forms via FGF20 primed cell cycle exit, cell motility, and aggregation. *ELife*, *7*, 1–33. https://doi.org/10.7554/eLife.36468

Bostock, M. P., Prasad, A. R., Chaouni, R., Yuen, A. C., Sousa-Nunes, R., Amoyel, M., & Fernandes, V. M. (2020). An Immobilization Technique for Long-Term Time-Lapse Imaging of Explanted Drosophila Tissues. *Frontiers in Cell and Developmental Biology*, *8*. https://doi.org/10.3389/fcell.2020.590094

Boulais, P. E., & Frenette, P. S. (2015). *Review Series Making sense of hematopoietic stem cell niches*. https://doi.org/10.1182/blood-2014

Boulet, M., Renaud, Y., Lapraz, F., Benmimoun, B., Vandel, L., & Waltzer, L. (2021). Characterization of the Drosophila Adult Hematopoietic System Reveals a Rare Cell Population With Differentiation and Proliferation Potential. *Frontiers in Cell and Developmental Biology*, *9*. https://doi.org/10.3389/fcell.2021.739357

Bunt, S., Hooley, C., Hu, N., Scahill, C., Weavers, H., & Skaer, H. (2010). Hemocyte-secreted type IV collagen enhances BMP signaling to guide renal tubule morphogenesis in Drosophila. *Developmental Cell*, *19*(2), 296–306. https://doi.org/10.1016/j.devcel.2010.07.019

Chakkalakal, J. V., Jones, K. M., Basson, M. A., & Brack, A. S. (2012). The aged niche disrupts muscle stem cell quiescence. *Nature*, *490*(7420), 355–360. https://doi.org/10.1038/nature11438

Cho, B., Yoon, S. H., Lee, D., Koranteng, F., Tattikota, S. G., Cha, N., Shin, M., Do, H., Hu, Y., Oh, S. Y., Lee, D., Vipin Menon, A., Moon, S. J., Perrimon, N., Nam, J. W., & Shim, J. (2020). Single-cell transcriptome maps of myeloid blood cell lineages in Drosophila. *Nature Communications*, *11*(1). https://doi.org/10.1038/s41467-020-18135-y

Cliffe, A., Doupé, D. P., Sung, H., Lim, I. K. H., Ong, K. H., Cheng, L., & Yu, W. (2017). Quantitative 3D analysis of complex single border cell behaviors in coordinated collective cell migration. *Nature Communications*, *8*. https://doi.org/10.1038/ncomms14905

Crozatier, M., Ubeda, J. M., Vincent, A., & Meister, M. (2004). Cellular immune response to parasitization in Drosophila requires the EBF orthologue collier. *PLoS Biology*, *2*(8). https://doi.org/10.1371/journal.pbio.0020196

Dalle Nogare, D. E., Natesh, N., Vishwasrao, H. D., Shroff, H., & Chitnis, A. B. (2020). Zebrafish Posterior Lateral Line primordium migration requires interactions between a superficial sheath of motile cells and the skin. *ELife*, *9*. https://doi.org/10.7554/eLife.58251

de Cuevas, M., & Spradling, A. (1998). Morphogenesis of the Drosophila fusome and its implications for oocyte specification. *Development*, *125*(15). https://doi.org/10.1242/dev.125.15.2781

Destalminil-Letourneau, M., Morin-Poulard, I., Tian, Y., Vanzo, N., & Crozatier, M. (2021). The vascular niche controls drosophila hematopoiesis via fibroblast growth factor signaling. *ELife*, *10*, 1–21. https://doi.org/10.7554/eLife.64672

Díaz-Torres, A., Rosales-Nieves, A. E., Pearson, J. R., Santa-Cruz Mateos, C., Marín-Menguiano, M., Marshall, O. J., Brand, A. H., & González-Reyes, A. (2021). Stem cell niche organization in the Drosophila ovary requires the ECM component Perlecan. *Current Biology*, *31*(8), 1744-1753.e5. https://doi.org/10.1016/j.cub.2021.01.071

Englund, C., Lorén, C. E., Grabbe, C., Varshney, G. K., Deleuil, F., Hallberg, B., & Palmer, R. H. (2003). Jeb signals through the Alk receptor tyrosine kinase to drive visceral muscle fusion. *Nature*, *425*(6957), 512–516. https://doi.org/10.1038/nature01950

Englund, C., Steneberg, P., Falileeva, L., Xylourgidis, N., & Samakovlis, C. (2002). Attractive and repulsive functions of Slit are mediated by different receptors in the *Drosophila* trachea. *Development*, *129*(21), 4941–4951. https://doi.org/10.1242/dev.129.21.4941

Ferraro, F., Lo Celso, C., & Scadden, D. (2010). Adult stem cells and their niches. In *Advances in Experimental Medicine and Biology* (Vol. 695, pp. 155–168). https://doi.org/10.1007/978-1-4419-7037-4_11

Gajewski, K., Choi, C. Y., Kim, Y., & Schulz, R. A. (2000). Genetically distinct cardial cells within the Drosophila heart. *Genesis*, *28*(1), 36–43. https://doi.org/10.1002/1526-968X(200009)28:1<36::AID-GENE50>3.0.CO;2-4

Girard, J. R., Goins, L. M., Vuu, D. M., Sharpley, M. S., Spratford, C. M., Mantri, S. R., & Banerjee, U. (2021). *Paths and pathways that generate cell-type heterogeneity and developmental progression in hematopoiesis*. *10*. https://doi.org/10.7554/eLife

Gordon, K. L., Zussman, J. W., Li, X., Miller, C., & Sherwood, D. R. (2020). Stem cell niche exit in C. Elegans via orientation and segregation of daughter cells by a cryptic cell outside the niche. *ELife*, *9*, 1–56. https://doi.org/10.7554/eLife.56383

Gregg, C. L., & Butcher, J. T. (2012). Quantitative in vivo imaging of embryonic development: Opportunities and challenges. In *Differentiation* (Vol. 84, Issue 1, pp. 149–162). https://doi.org/10.1016/j.diff.2012.05.003

Grigorian, M., Mandal, L., & Hartenstein, V. (2011). Hematopoiesis at the onset of metamorphosis: terminal differentiation and dissociation of the Drosophila lymph gland. *Development Genes and Evolution*, *221*(3), 121–131. https://doi.org/10.1007/s00427-011-0364-6

Gupta, K., Levinsohn, J., Linderman, G., Chen, D., Sun, T. Y., Dong, D., Taketo, M. M., Bosenberg, M., Kluger, Y., Choate, K., & Myung, P. (2019). Single-Cell Analysis Reveals a Hair Follicle Dermal Niche Molecular Differentiation Trajectory that Begins Prior to Morphogenesis. *Developmental Cell*, *48*(1), 17-31.e6. https://doi.org/10.1016/j.devcel.2018.11.032

Haas, P., & Gilmour, D. (2006). Chemokine Signaling Mediates Self-Organizing Tissue Migration in the Zebrafish Lateral Line. *Developmental Cell*, *10*(5), 673–680. https://doi.org/10.1016/j.devcel.2006.02.019

Han, Z., & Bodmer, R. (2003). Myogenic cells fates are antagonized by Notch only in asymmetric lineages of the Drosophila heart, with or without cell division. *Development*, *130*(13), 3039–3051. https://doi.org/10.1242/dev.00484

Hartenstein, V. (1993). *Atlas of Drosophila Development* (Issue v. 328). Cold Spring Harbor Laboratory Press. https://books.google.com/books?id=A6vwAAAAMAAJ

Heitman, N., Saxena, N., & Rendl, M. (2018). Advancing insights into stem cell niche complexities with next-generation technologies. In *Current Opinion in Cell Biology* (Vol. 55, pp. 87–95). Elsevier Ltd. https://doi.org/10.1016/j.ceb.2018.06.012

Hirschhäuser, A., Molitor, D., Salinas, G., Großhans, J., Rust, K., & Bogdan, S. (2023). Single-cell transcriptomics identifies new blood cell populations in Drosophila released at the onset of metamorphosis. *Development (Cambridge)*, *150*(18). https://doi.org/10.1242/dev.201767

Ho, K. Y. L., An, K., Carr, R. L., Dvoskin, A. D., Ou, A. Y. J., Vogl, W., & Tanentzapf, G. (2023). Maintenance of hematopoietic stem cell niche homeostasis requires gap junction–mediated calcium signaling. *Proceedings of the National Academy of Sciences of the United States of America*, *120*(45). https://doi.org/10.1073/pnas.2303018120

Ho, K. Y. L., Khadilkar, R. J., Carr, R. L., & Tanentzapf, G. (2021). A gap-junction-mediated, calcium-signaling network controls blood progenitor fate decisions in hematopoiesis. *Current Biology*, *31*(21), 4697-4712.e6. https://doi.org/10.1016/j.cub.2021.08.027

Holmberg, J., Genander, M., Halford, M. M., Annerén, C., Sondell, M., Chumley, M. J., Silvany, R. E., Henkemeyer, M., & Frisén, J. (2006). EphB Receptors Coordinate Migration and Proliferation in the Intestinal Stem Cell Niche. *Cell*, *125*(6), 1151–1163. https://doi.org/10.1016/j.cell.2006.04.030

Holz, A., Bossinger, B., Strasser, T., Janning, W., & Klapper, R. (2003). The two origins of hemocytes in *Drosophila*. *Development*, *130*(20), 4955–4962. https://doi.org/10.1242/dev.00702

Jenkins, V.K., Larkin, A., Thurmond, J., FlyBase Consortium, (2022). Using FlyBase: A Database of Drosophila Genes and Genetics. Methods Mol. Biol. 2540(): 1--34.

Jung, S. H., Evans, C. J., Uemura, C., & Banerjee, U. (2005). The Drosophila lymph gland as a developmental model of hematopoiesis. *Development*, *132*(11), 2521–2533. https://doi.org/10.1242/dev.01837

Kellermeyer, R., Heydman, L. M., Gillis, T., Mastick, G. S., Song, M., & Kidd, T. (2020). Proteolytic cleavage of Slit by the Tolkin protease converts an axon repulsion cue to an axon growth cue *in vivo*. *Development*. https://doi.org/10.1242/dev.196055

Khadilkar, R. J., Vogl, W., Goodwin, K., & Tanentzapf, G. (n.d.). *Modulation of occluding junctions alters the hematopoietic niche to trigger immune activation*. https://doi.org/10.7554/eLife.28081.001

Khadilkar, R. J., Vogl, W., Goodwin, K., & Tanentzapf, G. (2017). Modulation of occluding junctions alters the hematopoietic niche to trigger immune activation. *ELife*, *6*, 1–30. https://doi.org/10.7554/eLife.28081

Kidd, T., Bland, K. S., & Goodman, C. S. (1999). Slit Is the Midline Repellent for the Robo Receptor in Drosophila. *Cell*, *96*(6), 785–794. https://doi.org/10.1016/S0092-8674(00)80589-9

Kobielak, K., Stokes, N., De La Cruz, J., Polak, L., & Fuchs, E. (2007). *Loss of a quiescent niche but not follicle stem cells in the absence of bone morphogenetic protein signaling*. www.pnas.org/cgi/content/full/

Kolesnikov, T., & Beckendorf, S. K. (2005). NETRIN and SLIT guide salivary gland migration. *Developmental Biology*, *284*(1), 102–111. https://doi.org/10.1016/j.ydbio.2005.04.037

Koranteng, F., Cho, B., & Shim, J. (2022). Intrinsic and Extrinsic Regulation of Hematopoiesis in Drosophila. In *Molecules and Cells* (Vol. 45, Issue 3, pp. 101–108). Korean Society for Molecular and Cellular Biology. https://doi.org/10.14348/molcells.2022.2039

Kramer, S. G., Kidd, T., Simpson, J. H., & Goodman, C. S. (2001). Switching Repulsion to Attraction: Changing Responses to Slit During Transition in Mesoderm Migration. *Science*, *292*(5517), 737–740. https://doi.org/10.1126/science.1058766

Krzemień, J., Dubois, L., Makki, R., Meister, M., Vincent, A., & Crozatier, M. (2007). Control of blood cell homeostasis in Drosophila larvae by the posterior signalling centre. *Nature*, *446*(7133), 325–328. https://doi.org/10.1038/nature05650

Krzemien, J., Oyallon, J., Crozatier, M., & Vincent, A. (2010). Hematopoietic progenitors and hemocyte lineages in the Drosophila lymph gland. *Developmental Biology*, *346*(2), 310–319. https://doi.org/10.1016/j.ydbio.2010.08.003

Lanot, R., Zachary, D., Holder, F., & Meister, M. (2001). Postembryonic hematopoiesis in Drosophila. *Developmental Biology*, *230*(2), 243–257. https://doi.org/10.1006/dbio.2000.0123

Le Bras, S., & Van Doren, M. (2006). Development of the male germline stem cell niche in Drosophila. *Developmental Biology*, *294*(1), 92–103. https://doi.org/10.1016/j.ydbio.2006.02.030

Lebestky, T., Jung, S. H., & Banerjee, U. (2003). A Serrate-expressing signaling center controls Drosophila hematopoiesis. *Genes and Development*, *17*(3), 348–353. https://doi.org/10.1101/gad.1052803

Lee, H. H., Norris, A., Weiss, J. B., & Frasch, M. (2003). Jelly belly protein activates the receptor tyrosine kinase Alk to specify visceral muscle pioneers. *Nature*, *425*(6957), 507–512. https://doi.org/10.1038/nature01916

Lo, P. C. H., & Frasch, M. (2001). A role for the COUP-TF-related gene seven-up in the diversification of cardioblast identities in the dorsal vessel of Drosophila. *Mechanisms of Development*, *104*(1–2), 49–60. https://doi.org/10.1016/S0925-4773(01)00361-6

Louradour, I., Sharma, A., Morin-Poulard, I., Letourneau, M., Vincent, A., Crozatier, M., & Vanzo, N. (2017). Reactive oxygen species-dependent Toll/NF-κB activation in the drosophila hematopoietic niche confers resistance to wasp parasitism. *ELife*, *6*, 1–22. https://doi.org/10.7554/eLife.25496

Lucila Scimone, M., Cote, L. E., & Reddien, P. W. (2017). Orthogonal muscle fibres have different instructive roles in planarian regeneration. *Nature*, *551*(7682), 623–628. https://doi.org/10.1038/nature24660

Luo, F., Yu, S., & Jin, L. H. (2020). The Posterior Signaling Center Is an Important Microenvironment for Homeostasis of the Drosophila Lymph Gland. In *Frontiers in Cell and Developmental Biology* (Vol. 8). Frontiers Media S.A. https://doi.org/10.3389/fcell.2020.00382

MacMullin, A., & Jacobs, J. R. (2006a). Slit coordinates cardiac morphogenesis in Drosophila. *Developmental Biology*, *293*(1), 154–164. https://doi.org/10.1016/j.ydbio.2006.01.027

MacMullin, A., & Jacobs, J. R. (2006b). Slit coordinates cardiac morphogenesis in Drosophila. *Developmental Biology*, *293*(1), 154–164. https://doi.org/10.1016/j.ydbio.2006.01.027

Mandal, L., Banerjee, U., & Hartenstein, V. (2004). Evidence for a fruit fly hemangioblast and similarities between lymph-gland hematopoiesis in fruit fly and mammal aorta-gonadal-mesonephros mesoderm. *Nature Genetics*, *36*(9), 1019–1023. https://doi.org/10.1038/ng1404

Mandal, L., Martinez-Agosto, J. A., Evans, C. J., Hartenstein, V., & Banerjee, U. (2007). A Hedgehog- and Antennapedia-dependent niche maintains Drosophila haematopoietic precursors. *Nature*, *446*(7133), 320–324. https://doi.org/10.1038/nature05585

Medioni, C., Astier, M., Zmojdzian, M., Jagla, K., & Sémériva, M. (2008a). Genetic control of cell morphogenesis during Drosophila melanogaster cardiac tube formation. *Journal of Cell Biology*, *182*(2), 249–261. https://doi.org/10.1083/jcb.200801100

Medioni, C., Astier, M., Zmojdzian, M., Jagla, K., & Sémériva, M. (2008b). Genetic control of cell morphogenesis during Drosophila melanogaster cardiac tube formation. *Journal of Cell Biology*, *182*(2), 249–261. https://doi.org/10.1083/jcb.200801100

Morin-Poulard, I., Sharma, A., Louradour, I., Vanzo, N., Vincent, A., & Crozatier, M. (2016). Vascular control of the Drosophila haematopoietic microenvironment by Slit/Robo signalling. *Nature Communications*, *7*. https://doi.org/10.1038/ncomms11634

Morrison, S. J., & Spradling, A. C. (2008). Stem Cells and Niches: Mechanisms That Promote Stem Cell Maintenance throughout Life. In *Cell* (Vol. 132, Issue 4, pp. 598–611). Elsevier B.V. https://doi.org/10.1016/j.cell.2008.01.038

Peercy, B. E., & Starz-Gaiano, M. (2020). Clustered cell migration: Modeling the model system of Drosophila border cells. *Seminars in Cell & Developmental Biology*, *100*, 167–176. https://doi.org/10.1016/j.semcdb.2019.11.010

Pentinmikko, N., Lozano, R., Scharaw, S., Andersson, S., Englund, J. I., Castillo-Azofeifa, D., Gallagher, A., Broberg, M., Song, K.-Y., Sola Carvajal, A., Speidel, A. T., Sundstrom, M., Allbritton, N., Stevens, M. M., Klein, O. D., Teixeira, A., & Katajisto, P. (2022). Cellular shape reinforces niche to stem cell signaling in the small intestine. In *Sci. Adv* (Vol. 8). https://www.science.org

Pinho, S., & Frenette, P. S. (2019). Haematopoietic stem cell activity and interactions with the niche. In *Nature Reviews Molecular Cell Biology* (Vol. 20, Issue 5, pp. 303–320). Nature Publishing Group. https://doi.org/10.1038/s41580-019-0103-9

Qian, L., Liu, J., & Bodmer, R. (2005). Slit and Robo control cardiac cell polarity and morphogenesis. *Current Biology*, *15*(24), 2271–2278. https://doi.org/10.1016/j.cub.2005.10.037

Qin, L., Yang, D., Yi, W., Cao, H., & Xiao, G. (2021). Roles of leader and follower cells in collective cell migration. *Molecular Biology of the Cell*, *32*(14), 1267–1272. https://doi.org/10.1091/mbc.E20-10-0681

Ramesh, P., Dey, N. S., Kanwal, A., Mandal, S., & Mandal, L. (2021). Relish plays a dynamic role in the niche to modulate drosophila blood progenitor homeostasis in development and infection. *ELife*, *10*. https://doi.org/10.7554/eLife.67158

Raz, A. A., Vida, G. S., Stern, S. R., Mahadevaraju, S., Fingerhut, J. M., Viveiros, J. M., Pal, S., Grey, J. R., Grace, M. R., Berry, C. W., Li, H., Janssens, J., Saelens, W., Shao, Z., Hu, C., Yamashita, Y. M., Przytycka, T., Oliver, B., Brill, J. A., … Buszczak, M. (2023). *Emergent dynamics of adult stem cell lineages from single nucleus and single cell RNA-Seq of Drosophila testes*. *12*, 82201. https://doi.org/10.7554/eLife

Rizki, T. M., & Rizki, R. M. (1992). Lamellocyte differentiation in Drosophila larvae parasitized by Leptopilina. *Developmental & Comparative Immunology*, *16*(2–3), 103–110. https://doi.org/10.1016/0145-305X(92)90011-Z

Rompolas, P., Mesa, K. R., & Greco, V. (2013). Spatial organization within a niche as a determinant of stem-cell fate. *Nature*, *502*(7472), 513–518. https://doi.org/10.1038/nature12602

Rothberg, J. M., Hartley, D. A., Walther, Z., & Artavanis-Tsakonas, S. (1988). slit: An EGF-homologous locus of D. melanogaster involved in the development of the embryonic central nervous system. *Cell*, *55*(6), 1047–1059. https://doi.org/10.1016/0092-8674(88)90249-8

Rothberg, J. M., Jacobs,^'^, / J Roger, Goodman, C. S., & Artavanis-Tsakonas, S. (1990). *slit: an extracellular protein necessary for development of midline glia and commissural axon pathways contains both EGF and LRR domains*.

988 Santiago-Martínez, E., Soplop, N. H., & Kramer, S. G. (2006). *Lateral positioning at the dorsal midline: Slit and*
989 *Roundabout receptors guide Drosophila heart cell migration*.
990 www.pnas.orgcgidoi10.1073pnas.0605284103

991 Santiago-Martínez, E., Soplop, N. H., Patel, R., & Kramer, S. G. (2008). Repulsion by Slit and Roundabout
992 prevents Shotgun/E-cadherin-mediated cell adhesion during Drosophila heart tube lumen formation.
993 *Journal of Cell Biology*, *182*(2), 241–248. https://doi.org/10.1083/jcb.200804120

994 SHRESTHA, R., & GATEFF, E. (1982). Ultrastructure and Cytochemistry of the Cell Types in the Larval
995 Hematopoietic Organs and Hemolymph of Drosophila Melanogaster drosophila/hematopoiesis/blool
996 cells/ultrastructure/cytochemistry. *Development, Growth & Differentiation*, *24*(1), 65–82.
997 https://doi.org/10.1111/j.1440-169X.1982.00065.x

998 Sinenko, S. A., Mandal, L., Martinez-Agosto, J. A., & Banerjee, U. (2009). Dual Role of Wingless Signaling in
999 Stem-like Hematopoietic Precursor Maintenance in Drosophila. *Developmental Cell*, *16*(5), 756–763.
000 https://doi.org/10.1016/j.devcel.2009.03.003

001 Sinenko, S. A., Shim, J., & Banerjee, U. (2012). Oxidative stress in the haematopoietic niche regulates the
002 cellular immune response in Drosophila. *EMBO Reports*, *13*(1), 83–89.
003 https://doi.org/10.1038/embor.2011.223

004 Spéder, P., & Brand, A. H. (2018). Systemic and local cues drive neural stem cell niche remodelling during
005 neurogenesis in Drosophila. *ELife*. https://doi.org/10.7554/eLife.30413.001

006 Spratford, C. M., Goins, L. M., Chi, F., Girard, J. R., Macias, S. N., Ho, V. W., & Banerjee, U. (2021). Intermediate
007 progenitor cells provide a transition between hematopoietic progenitors and their differentiated
008 descendants. *Development (Cambridge)*, *148*(24). https://doi.org/10.1242/dev.200216

009 Sumigray, K. D., Terwilliger, M., & Lechler, T. (2018). Morphogenesis and Compartmentalization of the Intestinal
010 Crypt. *Developmental Cell*, *45*(2), 183-197.e5. https://doi.org/10.1016/j.devcel.2018.03.024

011 Tian, Y., Morin-Poulard, I., Liu, X., Vanzo, N., & Crozatier, M. (2023). A mechanosensitive vascular niche for
012 Drosophila hematopoiesis. *Proceedings of the National Academy of Sciences of the United States of*
013 *America*, *120*(118). https://doi.org/10.1073/pnas.2217862120

014 Tokusumi, T., Tokusumi, Y., Hopkins, D. W., & Schulz, R. A. (2015). Bag of Marbles controls the size and
015 organization of the Drosophila hematopoietic niche through interactions with the Insulin-like growth
016 factor pathway and Retinoblastoma-family protein. *Development (Cambridge)*, *142*(13), 2261–2267.
017 https://doi.org/10.1242/dev.121798

018 van Es, J. H., Jay, P., Gregorieff, A., van Gijn, M. E., Jonkheer, S., Hatzis, P., Thiele, A., van den Born, M., Begthel,
019 H., Brabletz, T., Taketo, M. M., & Clevers, H. (2005). Wnt signalling induces maturation of Paneth cells in
020 intestinal crypts. *Nature Cell Biology*, *7*(4), 381–386. https://doi.org/10.1038/ncb1240

021 Walkley, C. R., Olsen, G. H., Dworkin, S., Fabb, S. A., Swann, J., McArthur, G. A. A., Westmoreland, S. V.,
022 Chambon, P., Scadden, D. T., & Purton, L. E. (2007). A Microenvironment-Induced Myeloproliferative
023 Syndrome Caused by Retinoic Acid Receptor γ Deficiency. *Cell*, *129*(6), 1097–1110.
024 https://doi.org/10.1016/j.cell.2007.05.014

Ward, E. J., & Skeath, J. B. (2000). Characterization of a novel subset of cardiac cells and their progenitors in the Drosophila embryo. *Development*, *127*(22). https://doi.org/10.1242/dev.127.22.4959

Warder, B. N., Nelson, K. A., Sui, J., Anllo, L., & Dinardo, S. (2024). An actomyosin network organizes niche morphology and responds to feedback from recruited stem cells. *BioRxiv*. https://doi.org/10.1101/2023.09.08.556877

Weavers, H., & Skaer, H. (2013). Tip Cells Act as Dynamic Cellular Anchors in the Morphogenesis of Looped Renal Tubules in Drosophila. *Developmental Cell*, *27*(3), 331–344. https://doi.org/10.1016/j.devcel.2013.09.020

Weiss, J. B., Suyama, K. L., Lee, H. H., & Scott, M. P. (2001). Jelly belly: A Drosophila LDL receptor repeat-containing signal required for mesoderm migration and differentiation. *Cell*, *107*(3), 387–398. https://doi.org/10.1016/S0092-8674(01)00540-2

Witchley, J. N., Mayer, M., Wagner, D. E., Owen, J. H., & Reddien, P. W. (2013). Muscle cells provide instructions for planarian regeneration. *Cell Reports*, *4*(4), 633–641. https://doi.org/10.1016/j.celrep.2013.07.022

Zaffran, S., Küchler, A., Lee, H. H., & Frasch, M. (2001). biniou (FoxF), a central component in a regulatory network controlling visceral mesoderm development and midgut morphogenesis in Drosophila. *Genes and Development*, *15*(21), 2900–2915. https://doi.org/10.1101/gad.917101

Zhang, J., Niu, C., Ye, L., Huang, H., He, X., Tong, W. G., Ross, J., Haug, J., Johnson, T., Feng, J. Q., Harris, S., Wiedemann, L. M., Mishina, Y., & Li, L. (2003). Identification of the haematopoietic stem cell niche and control of the niche size. *Nature*, *425*(6960), 836–841. https://doi.org/10.1038/nature02041

Zheng, Q., Wang, Y., Vargas, E., & DiNardo, S. (2011). Magu is required for germline stem cell self-renewal through BMP signaling in the Drosophila testis. *Developmental Biology*, *357*(1), 202–210. https://doi.org/10.1016/j.ydbio.2011.06.022

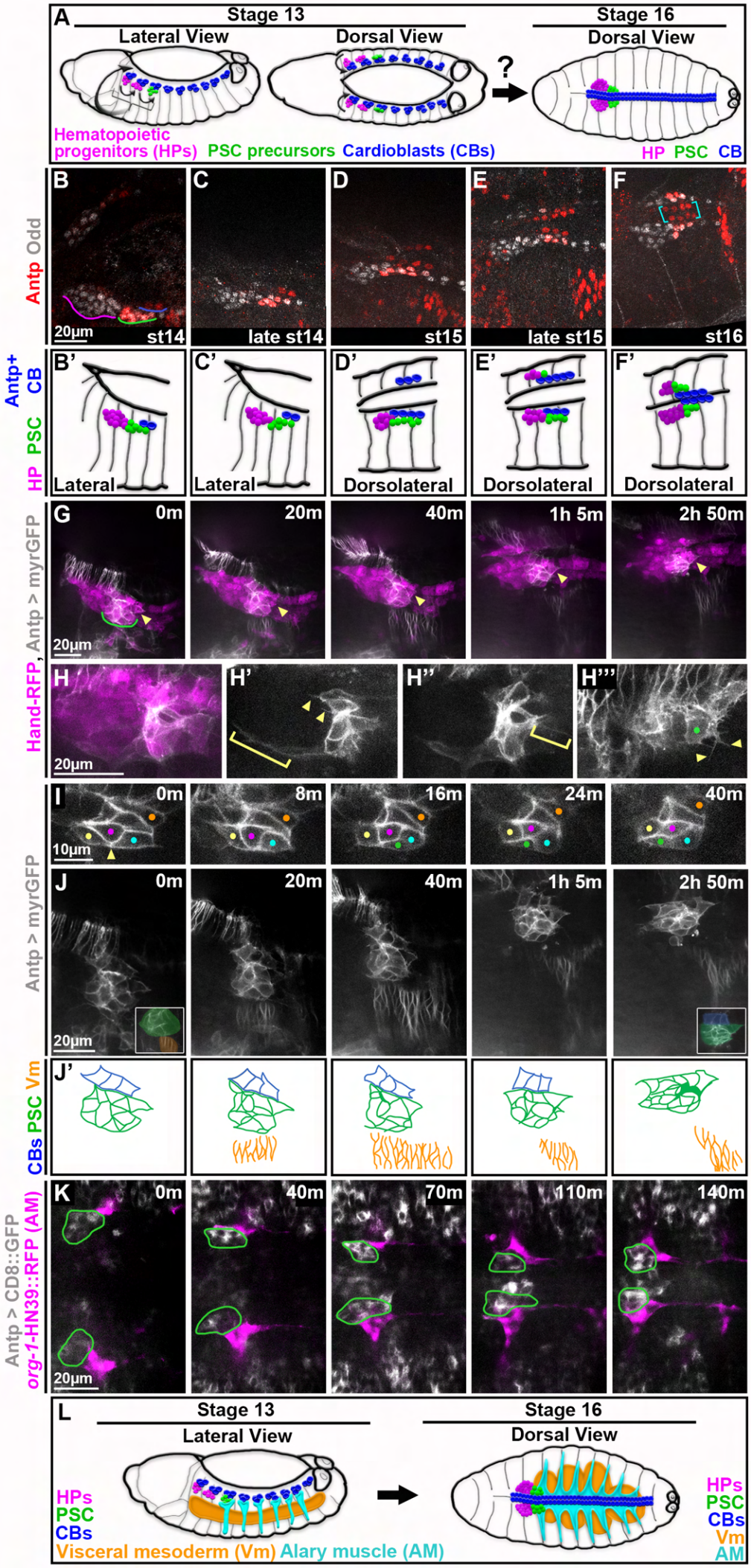
A
Stage 13
Lateral View
Dorsal View
Stage 16
Dorsal View
?
Hematopoietic progenitors (HPs)
PSC precursors
Cardioblasts (CBs)
HP PSC CB
Antp Odd
B
C
D
E
F
20µm
st14
late st14
st15
late st15
st16
Antp+ CB
HP PSC
B'
C'
D'
E'
F'
Lateral
Lateral
Dorsolateral
Dorsolateral
Dorsolateral
Antp > myrGFP
G
0m
20m
40m
1h 5m
2h 50m
20µm
Hand-RFP
H
H'
H''
H'''
20µm
Antp > myrGFP
I
0m
8m
16m
24m
40m
10µm
J
0m
20m
40m
1h 5m
2h 50m
20µm
CBs PSC Vm
J'
Antp > CD8::GFP
org-1-HN39::RFP (AM)
K
0m
40m
70m
110m
140m
20µm
L
Stage 13
Lateral View
Stage 16
Dorsal View
HPs
PSC
CBs
Visceral mesoderm (Vm)
Alary muscle (AM)
HPs
PSC
CBs
Vm
AM

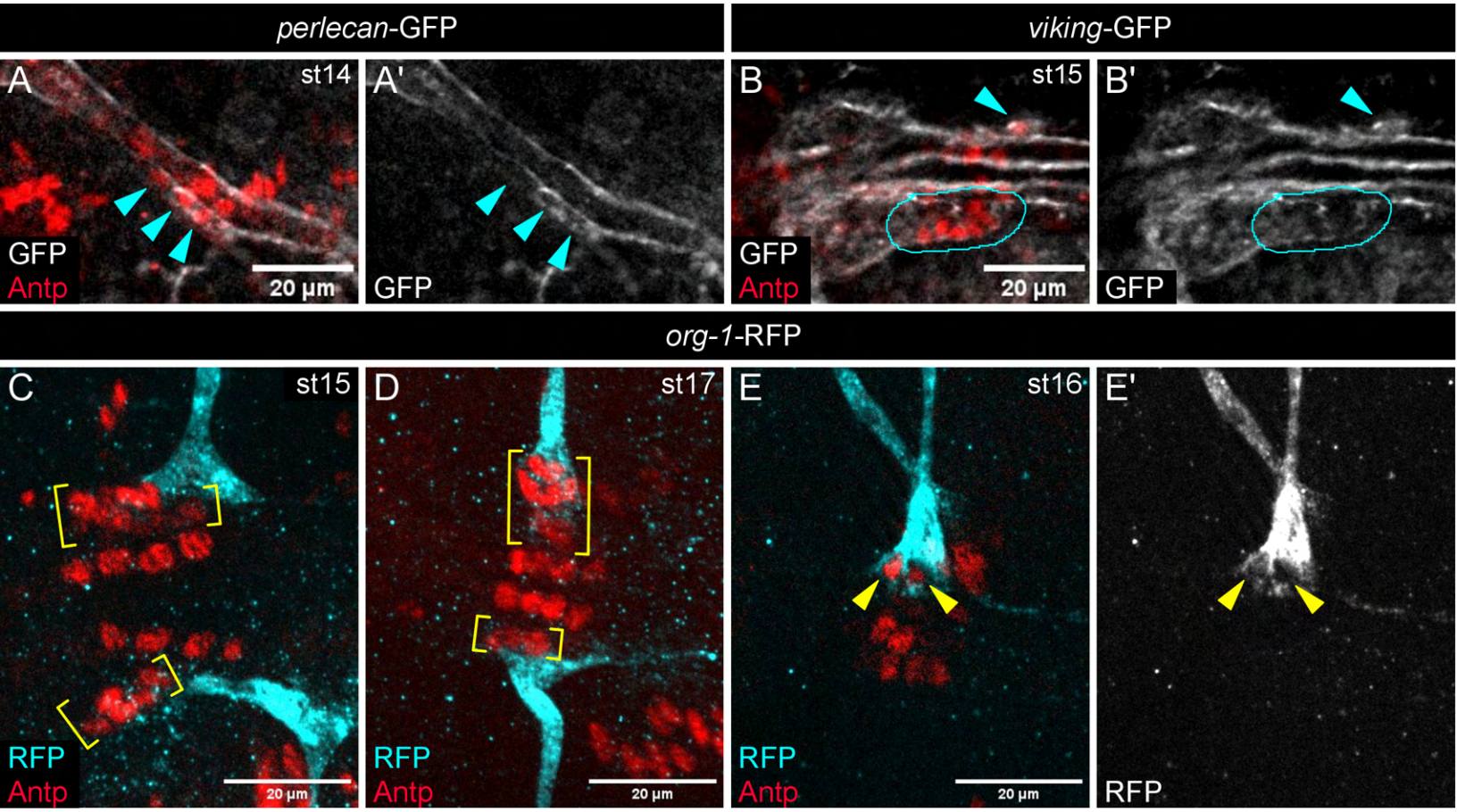
perlecan-GFP
viking-GFP
A
st14
A'
B
st15
B'
GFP
Antp
20 µm
GFP
GFP
Antp
20 µm
GFP
org-1-RFP
C
st15
D
st17
E
st16
E'
RFP
Antp
20 µm
RFP
Antp
20 µm
RFP
Antp
20 µm
RFP

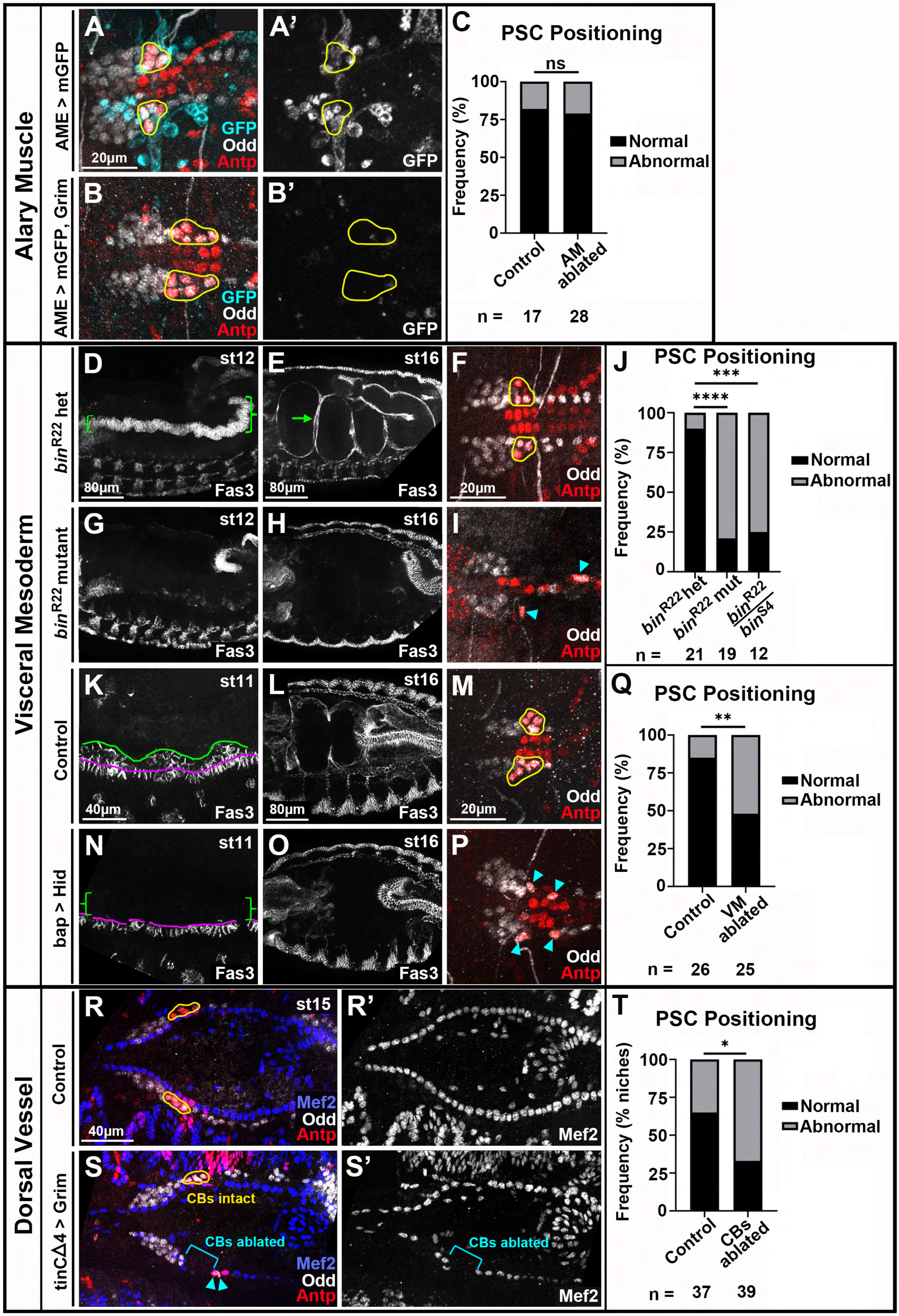
Alary Muscle
AME > mGFP
AME > mGFP, Grim
A
A'
B
B'
GFP
Odd
Antp
20µm
C
PSC Positioning
ns
Frequency (%)
Normal
Abnormal
Control
AM ablated
n = 17 28
Visceral Mesoderm
bin^R22 het
bin^R22 mutant
Control
bap > Hid
D
E
F
G
H
I
K
L
M
N
O
P
st12
st16
st11
Fas3
80µm
40µm
J
PSC Positioning
***
****
bin^R22 het
bin^R22 mut
bin^R22/bin^S4
n = 21 19 12
Q
PSC Positioning
**
VM ablated
n = 26 25
Dorsal Vessel
Control
tinCΔ4 > Grim
R
R'
S
S'
st15
Mef2
CBs intact
CBs ablated
T
PSC Positioning
*
Frequency (% niches)
CBs ablated
n = 37 39

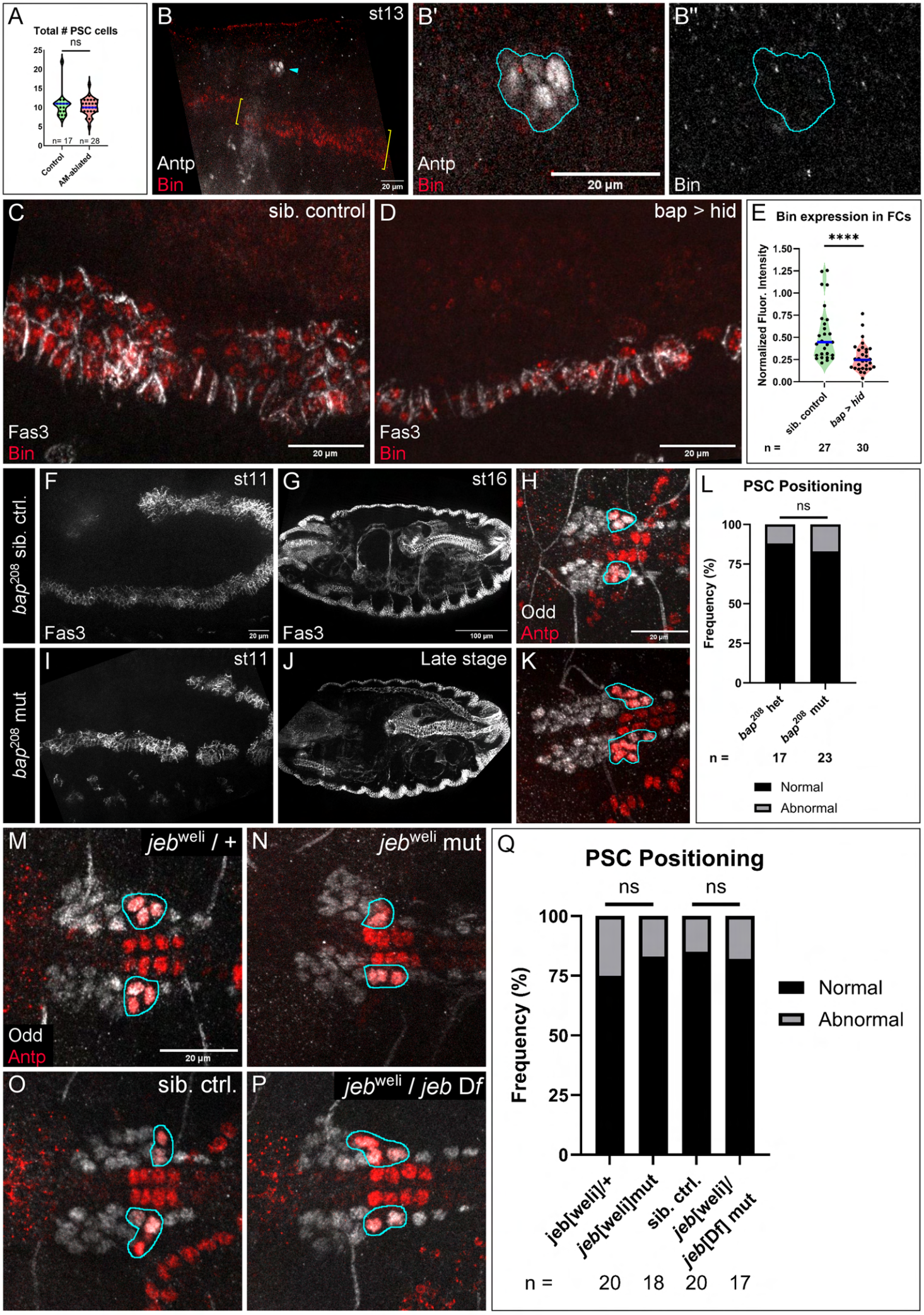
A
Total # PSC cells
ns
n= 17
n= 28
Control
AM-ablated
B
st13
Antp
Bin
20 µm
B'
Antp
Bin
20 µm
B''
Bin
C
sib. control
Fas3
Bin
20 µm
D
bap > hid
Fas3
Bin
20 µm
E
Bin expression in FCs
****
Normalized Fluor. Intensity
sib. control
bap > hid
n =
27
30
bap208 sib. ctrl.
F
st11
Fas3
20 µm
G
st16
Fas3
100 µm
H
Odd
Antp
20 µm
bap208 mut
I
st11
J
Late stage
K
L
PSC Positioning
ns
Frequency (%)
bap208 het
bap208 mut
n =
17
23
Normal
Abnormal
M
jebweli / +
Odd
Antp
20 µm
N
jebweli mut
O
sib. ctrl.
P
jebweli / jeb Df
Q
PSC Positioning
ns
ns
Frequency (%)
Normal
Abnormal
jeb[weli]/+
jeb[weli]mut
sib. ctrl.
jeb[weli]/
jeb[Df] mut
n =
20
18
20
17

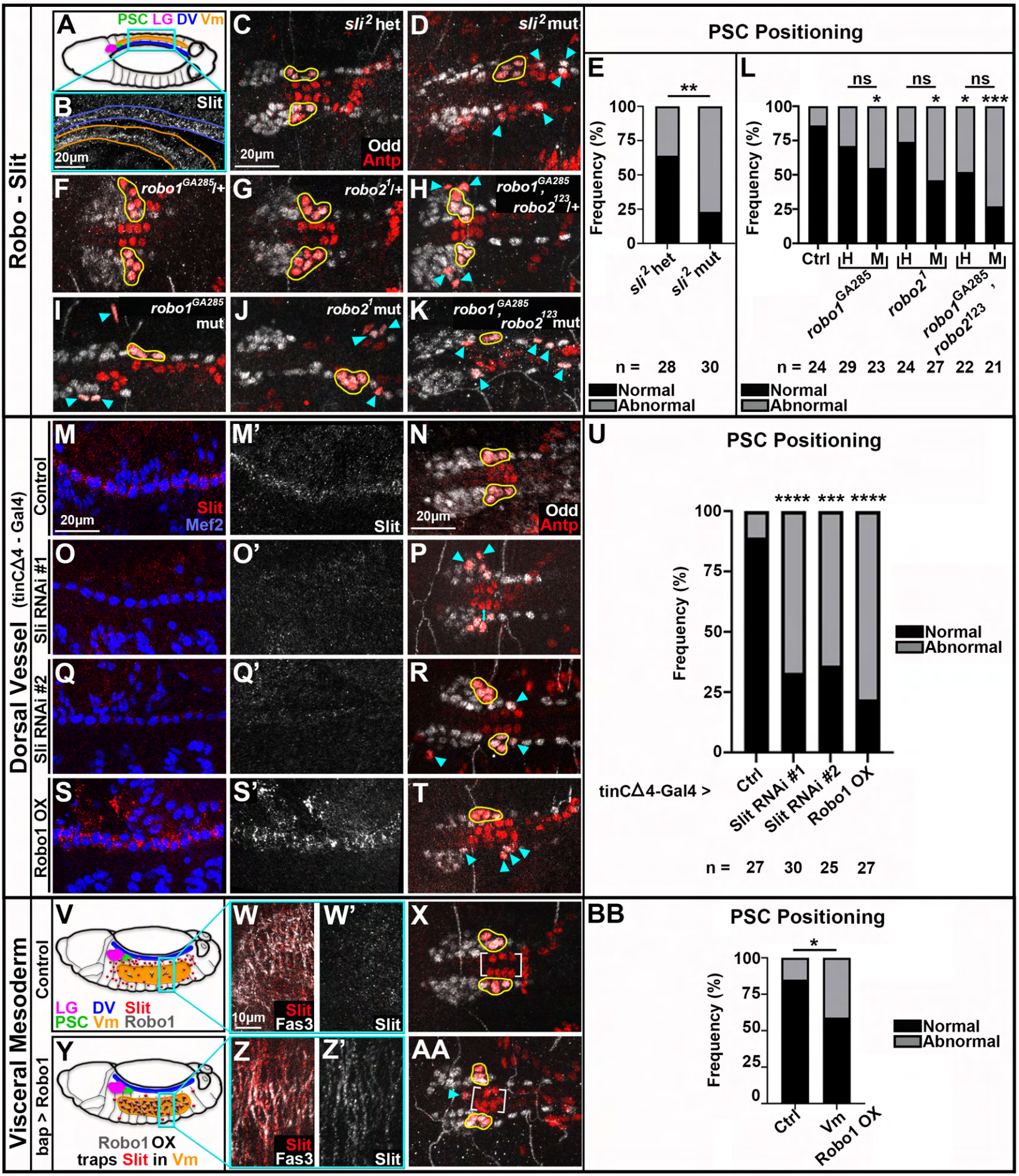
Robo - Slit
A
PSC LG DV Vm
B
Slit
20µm
C
sli2 het
20µm
Odd
Antp
D
sli2 mut
F
robo1GA285/+
G
robo2 1/+
H
robo1,GA285
robo2 123/+
I
robo1GA285
mut
J
robo2 1 mut
K
robo1,GA285
robo2 123 mut
PSC Positioning
E
Frequency (%)
100
75
50
25
0
**
sli2 het
sli2 mut
n = 28 30
Normal
Abnormal
L
ns
ns
ns
*
*
*
***
Ctrl
H
M
H
M
H
M
robo1GA285
robo2 1
robo1GA285,
robo2 123
n = 24 29 23 24 27 22 21
Normal
Abnormal
Dorsal Vessel (tinCΔ4 - Gal4)
Control
Sli RNAi #1
Sli RNAi #2
Robo1 OX
M
20µm
Slit
Mef2
M'
Slit
N
20µm
Odd
Antp
O
O'
P
Q
Q'
R
S
S'
T
U
PSC Positioning
Frequency (%)
100
75
50
25
0
**** *** ****
Normal
Abnormal
tinCΔ4-Gal4 >
Ctrl
Slit RNAi #1
Slit RNAi #2
Robo1 OX
n = 27 30 25 27
Visceral Mesoderm
Control
bap > Robo1
V
LG DV Slit
PSC Vm Robo1
Y
Robo1 OX
traps Slit in Vm
W
10µm
Slit
Fas3
W'
Slit
X
Z
Slit
Fas3
Z'
Slit
AA
BB
PSC Positioning
Frequency (%)
100
75
50
25
0
*
Normal
Abnormal
Ctrl
Vm
Robo1 OX

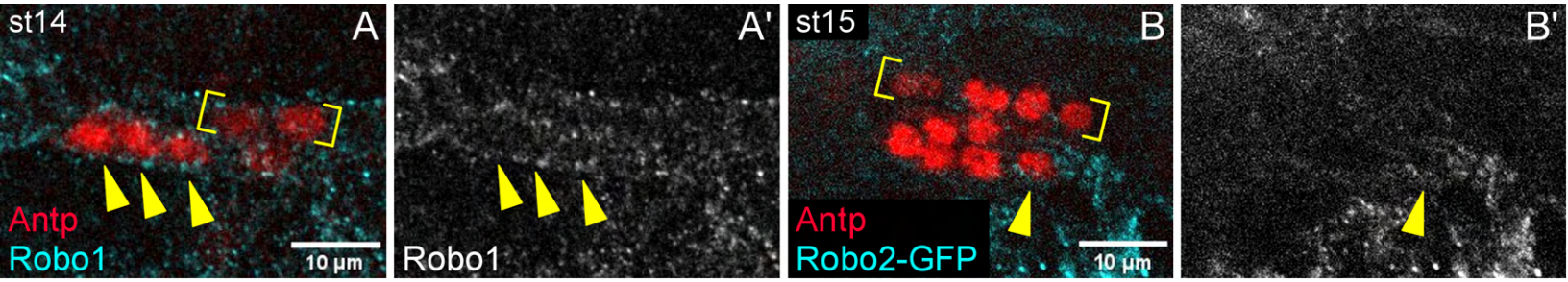
st14
A
Antp
Robo1
10 µm
A'
Robo1
st15
B
Antp
Robo2-GFP
10 µm
B'

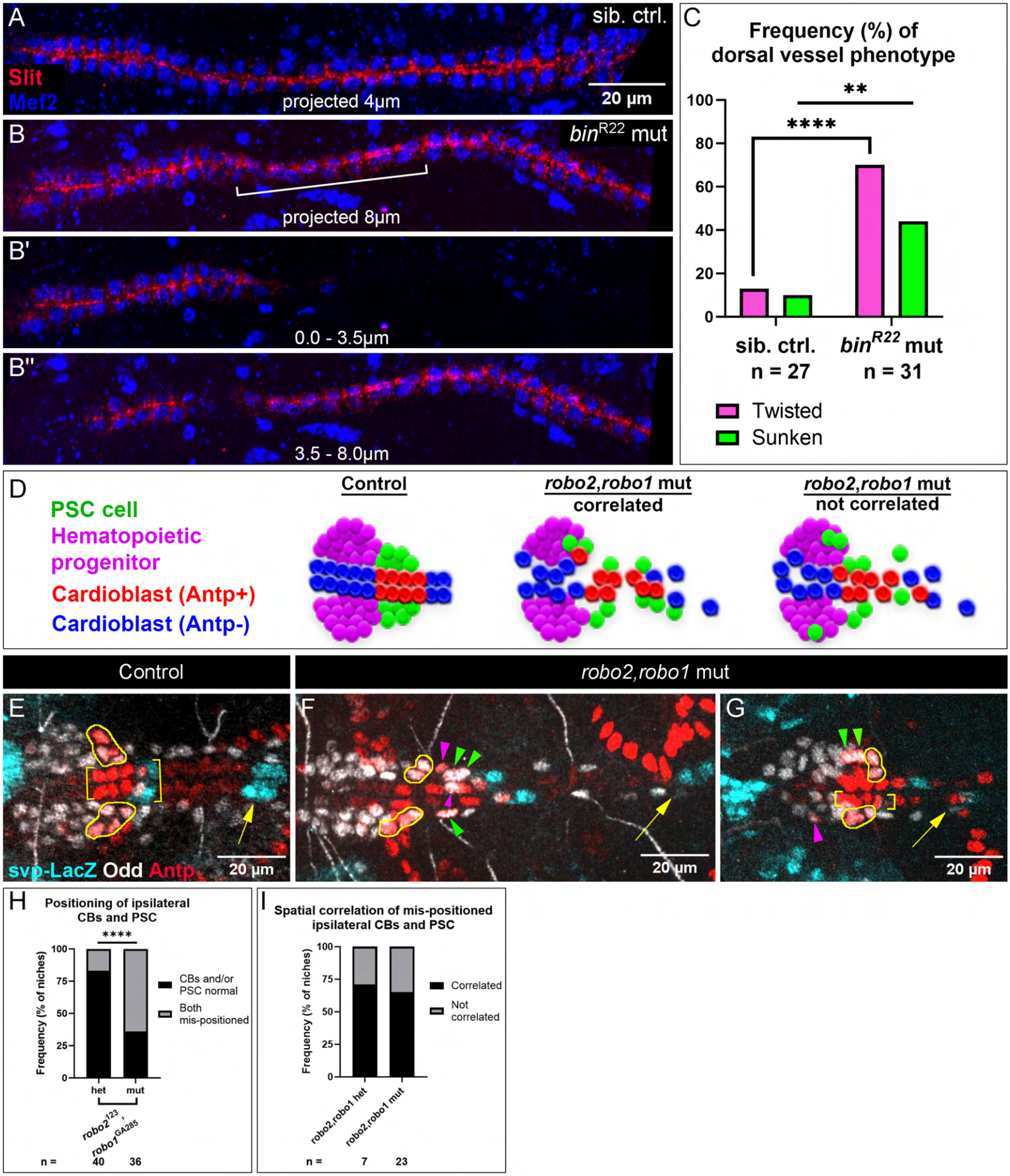
A
sib. ctrl.
Slit
Mef2
projected 4µm
20 µm
B
bin^R22 mut
projected 8µm
B'
0.0 - 3.5µm
B''
3.5 - 8.0µm
C
Frequency (%) of dorsal vessel phenotype
**
****
100
80
60
40
20
0
sib. ctrl. n = 27
bin^R22 mut n = 31
Twisted
Sunken
D
PSC cell
Hematopoietic progenitor
Cardioblast (Antp+)
Cardioblast (Antp-)
Control
robo2,robo1 mut correlated
robo2,robo1 mut not correlated
Control
robo2,robo1 mut
E
F
G
svp-LacZ Odd Antp
20 µm
20 µm
20 µm
H
Positioning of ipsilateral CBs and PSC
****
Frequency (% of niches)
100
75
50
25
0
CBs and/or PSC normal
Both mis-positioned
het
mut
robo2^123, robo1^GA285
n = 40 36
I
Spatial correlation of mis-positioned ipsilateral CBs and PSC
Frequency (% of niches)
100
75
50
25
0
Correlated
Not correlated
robo2,robo1 het
robo2,robo1 mut
n = 7 23

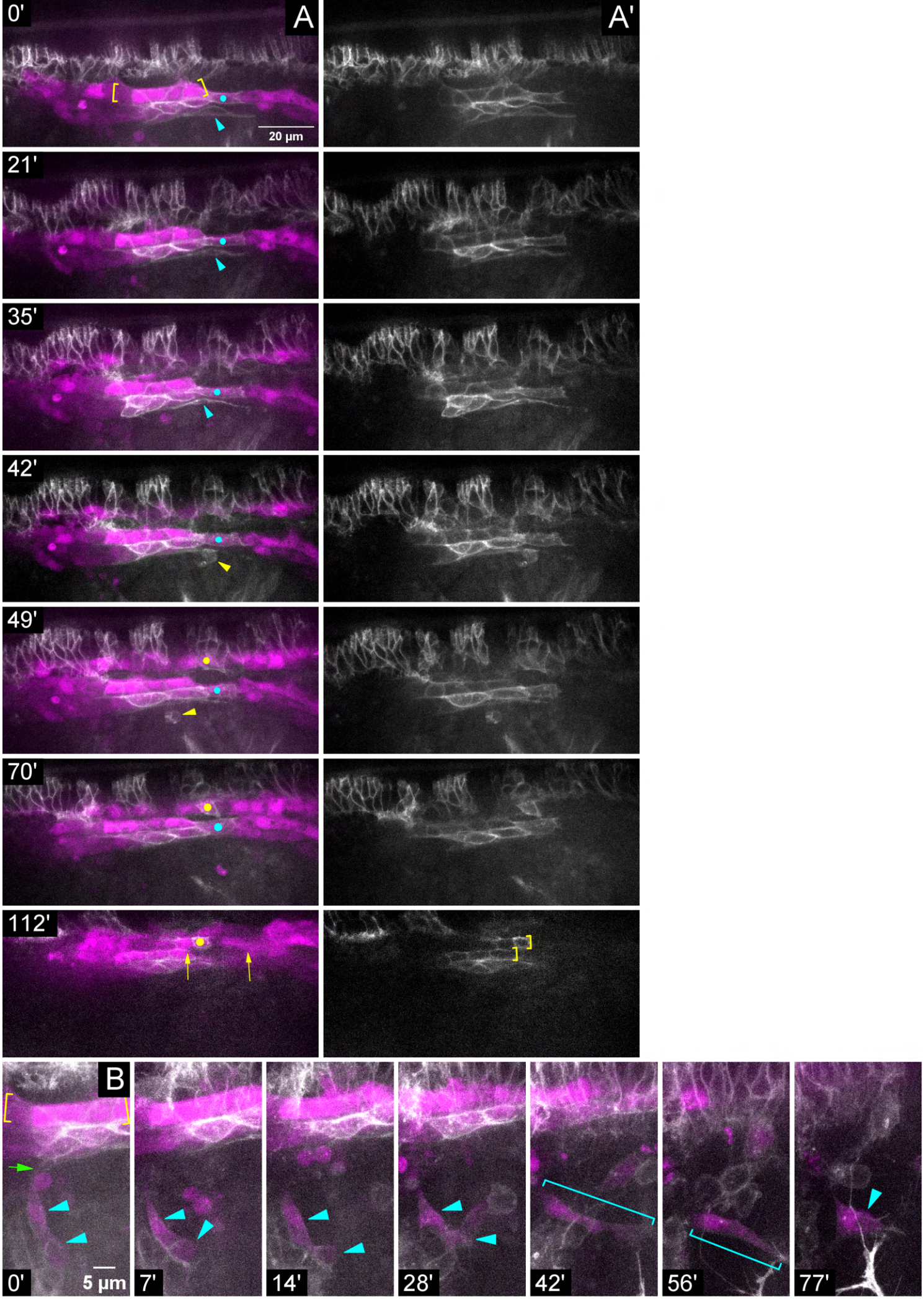
0'
A
A'
20 µm
21'
35'
42'
49'
70'
112'
B
0'
5 µm
7'
14'
28'
42'
56'
77'

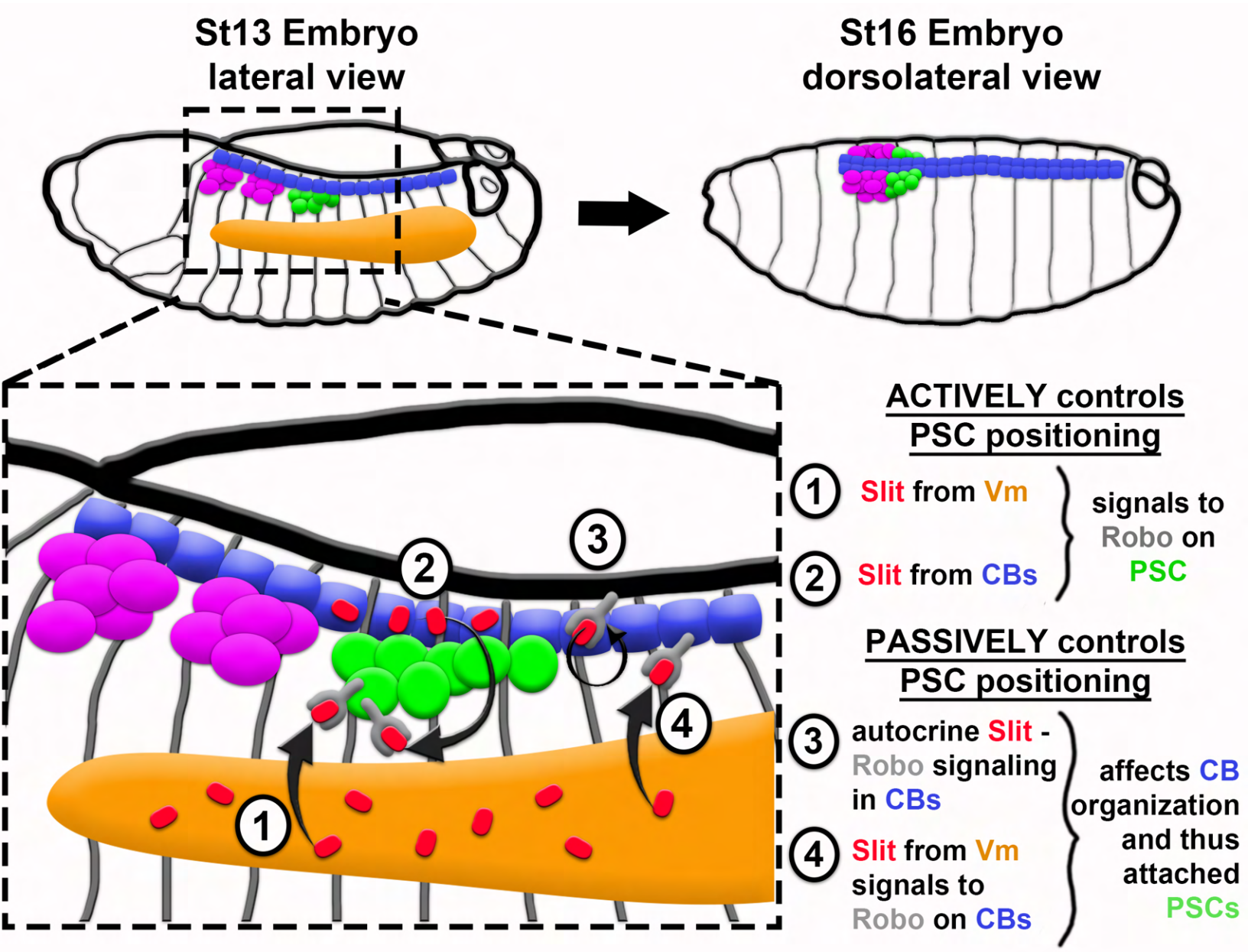
St13 Embryo
lateral view
St16 Embryo
dorsolateral view
ACTIVELY controls
PSC positioning
1 Slit from Vm
2 Slit from CBs
signals to
Robo on
PSC
PASSIVELY controls
PSC positioning
3 autocrine Slit -
Robo signaling
in CBs
4 Slit from Vm
signals to
Robo on CBs
affects CB
organization
and thus
attached
PSCs

1

Key Resources Table				
Reagent type (species) or resource	**Designation**	**Source or reference**	**Identifiers**	**Additional information**
genetic reagent (*D. melanogaster*)	Antp-GAL4	Emerald and Cohen, 2004	FLYB:FBal0155891	FlyBase symbol: GAL4$^{Antp-21}$
genetic reagent (*D. melanogaster*)	*w*^{1118}	Bloomington *Drosophila* Stock Center	BDSC:3605; FLYB:FBal0018186; RRID:BDSC_3605	FlyBase symbol: w^{1118}
genetic reagent (*D. melanogaster*)	Hand-RFP	other		Gift from Georg Vogler
genetic reagent (*D. melanogaster*)	UAS-myr:GFP	Bloomington *Drosophila* Stock Center	BDSC:32200; FLYB:FBti0131976 RRID:BDSC_32200	FlyBase symbol: P{10XUAS-IVS-myr::GFP}su(Hw)attP1
genetic reagent (*D. melanogaster*)	tupAME-GAL4	Bataillé et al., 2020	FLYB: FBtp0142468	FlyBase symbol:P{tup-GAL4.AME-R} Gift from J.L. Frendo
genetic reagent (*D. melanogaster*)	UAS-CD8:GFP	other		Gift from J.L. Frendo
genetic reagent (*D. melanogaster*)	org-1-HN39-RFP	Schaub and Frasch, 2015	FLYB:FBal0276776	FlyBase symbol: RFP$^{org-1.HN39}$
genetic reagent (*D. melanogaster*)	UAS-grim	Hugo Bellen	FLYB:FBti0154788	Flybase symbol: Dmel\P{UAS-grim.Y}2

genetic reagent (*D. melanogaster*)	*bin*^{R22}	Zaffran and Frasch, 2001	FLYB:FBal0043738	Flybase symbol: Dmel\bin^{R22}
genetic reagent (*D. melanogaster*)	*bin*^{S4}	Zaffran and Frasch, 2001	FLYB:FBal0043739	Flybase symbol: Dmel\bin^{S4}
genetic reagent (*D. melanogaster*)	UAS-hid	Bloomington *Drosophila* Stock Center	BDSC:65403; FLYB:FBti0183136 RRID:BDSC_65403	Flybase symbol: Dmel\P{UAS-hid.Z}2
genetic reagent (*D. melanogaster*)	bap-GAL4	Zaffran and Frasch, 2001	BDSC:91540; FLYB:FBti0214156	Flybase symbol: Dmel\P{bap-GAL4.3}1.1
genetic reagent (*D. melanogaster*)	bap-GAL4	other		gift from Manfred Frasch; Chr: X
genetic reagent (*D. melanogaster*)	tinCΔ4-GAL4	Bloomington *Drosophila* Stock Center	BDSC:92965; FLYB:FBti0216630	Flybase symbol: Dmel\P{tinC-Gal4.Δ4}12a
genetic reagent (*D. melanogaster*)	*slit*^{2}	Bloomington *Drosophila* Stock Center	BDSC:3266 FLYB:FBal0015700	Flybase symbol:Dmel \sli^{2}
genetic reagent (*D. melanogaster*)	*robo1*^{GA285}	other	FLYB:FBal0032588	Gift from Greg Bashaw Flybase symbol:Dmel \robo1^{1}
genetic reagent (*D. melanogaster*)	*robo2*^{1}	Rajagopalan and Dickinson, 2000	FLYB:FBal0121562	Gift from Greg Bashaw Flybase symbol:Dmel \robo2^{1}
genetic reagent (*D. melanogaster*)	*robo2*^{123}	other	FLYB:FBal0123720	Gift from Greg Bashaw Flybase

				symbol:Dmel \robo2^{X123}
genetic reagent (*D. melanogaster*)	UAS-Slit RNAi #1	Vienna *Drosophila* Stock Center	VDRC:v108853 FLYB:FBti0159991	Flybase symbol: Dmel\P{KK100803}VIE-260B
genetic reagent (*D. melanogaster*)	UAS-Slit RNAi #2	Bloomington *Drosophila* Stock Center	BDSC:31468 FLYB:FBal0245521	Flybase symbol:Dmel \sli^{JF01229}
genetic reagent (*D. melanogaster*)	UAS-Robo1 OX	Evans and Bashaw, 2015	BDSC:97240 FLYB:FBal0316479	Flybase symbol:Dmel \robo1 ΔC.10xUAS.Tag: HA,Tag:SS(wg)
genetic reagent (*D. melanogaster*)	UAS-dcr2	Bloomington *Drosophila* Stock Center	BDSC:24650 FLYB:FBti0100275	Flybase symbol:Dmel \P{UAS-Dcr-2.D}2
genetic reagent (*D. melanogaster*)	UAS-dcr2	Bloomington *Drosophila* Stock Center	BDSC:24651 FLYB:FBti0100276	Flybase symbol:Dmel \P{UAS-Dcr-2.D}10
genetic reagent (*D. melanogaster*)	svp-lacZ	Bloomington *Drosophila* Stock Center	BDSC:7314 FLYB:FBti0002862	Flybase symbol: Dmel\P{HZ}svp^{3}
genetic reagent (*D. melanogaster*)	perlecan-GFP	Flytrap; GFP Protein Trap Database	FLYB:FBal0243609	Flybase symbol:Dmel \trol^{ZCL1700}
genetic reagent (*D. melanogaster*)	viking-GFP	Buszczak and Spradling, 2007	FLYB:FBal0211825	Flybase symbol:Dmel \vkg^{CC00791}
genetic reagent (*D. melanogaster*)	*bap*^{208}	Bloomington *Drosophila* Stock Center	BDSC:91539 FLYB:FBal0034201	Flybase symbol:Dmel \bap^{208}

genetic reagent (*D. melanogaster*)	*jeb*^{weli}	Stute and Holz, 2004	FLYB:FBal0159133	Flybase symbol:Dmel \jeb^{weli}
genetic reagent (*D. melanogaster*)	*jeb* Df	Bloomington *Drosophila* Stock Center	BDSC:26551 FLYB:FBab0045764	Flybase symbol:Df(2R)BSC699
genetic reagent (*D. melanogaster*)	robo2-GFP	Bloomington *Drosophila* Stock Center	BDSC:61774 FLYB:FBal0265307	Flybase symbol:Dmel \robo2^{MI04295}
antibody	anti-Antp (Mouse monoclonal)	Developmental Studies Hybridoma Bank	Cat#:8C11, RRID:AB_528083	IF(1:50)
antibody	anti-Odd skipped (Rabbit polyclonal)	Ward and Skeath, 2000		IF(1:400); gift from James Skeath
antibody	anti-GFP (Chick polyclonal)	Aves labs	Cat#:GFP-1020 RRID:AB_2307313	IF(1:1500)
antibody	anti-Fas3 (Mouse monoclonal)	Developmental Studies Hybridoma Bank	Cat#:7G10 RRID:AB_528238	IF(1:50)
antibody	anti-Mef2 (Rabbit polyclonal)	Developmental Studies Hybridoma Bank	Cat#:Mef2 RRID:AB_2892602	IF(1:1000)
antibody	anti-Slit (Mouse monoclonal)	Developmental Studies Hybridoma Bank	Cat#:C555.6D RRID:AB_528470	IF(1:200); gift from Greg Bashaw

antibody	anti-LacZ (Chick polyclonal)	Abcam	Cat#:ab9361 RRID:AB_307210	IF(1:1000)
antibody	anti-RFP (Rabbit polyclonal)	Abcam	Cat#:ab62341 RRID:AB_945213	IF(1:1000)
antibody	anti-Bin (Rabbit polyclonal)	other		IF(1:100); gift from Eileen Furlong
antibody	anti-Robo1 (Mouse monoclonal)	other		IF(1:200); gift from Greg Bashaw
antibody	anti-Odd skipped (Guinea pig polyclonal)	other		IF(1:1200); gift from John Reinitz
chemical compound, drug	Paraformaldehyde	Electron Microscopy Sciences	Cat#:15710	
chemical compound, drug	Propyl-gallate	Sigma Aldrich	PubChem Substance ID:24898394; SKU:P3130; CAS Number:121-79-9	
chemical compound, drug	Normal Donkey Serum	Jackson ImmunoResearch Labs Inc	Cat#:017-000-121 RRID:AB_2337258	
chemical compound, drug	Ringer's solution	other		Recipe from https://doi.org/10.1242/dev.125.15.2781

chemical compound, drug	Triton X-100	MilliporeSigma	CAS Number: 9036-19-5	
software, algorithm	FIJI	ImajeJ	RRID:SCR_002285	http://fiji.sc
software, algorithm	Photoshop	Adobe	RRID:SCR_014199	https://www.adobe.com/products/photoshop.html
software, algorithm	Prism	Graphpad	RRID:SCR_002798	v9.0.0-v10.0.0
software, algorithm	Axio-Vision Imaging Software	Zeiss		v4.8.1
software, algorithm	VisiView	Visitron		
software, algorithm	Metamorph Microscopy Automation and Image Analysis Software	Leica		v7.8.40
other	63x / 1.2 NA water immersion objective	Leica		
other	60x / 1.3 NA silicone immersion objective	Olympus		
other	AxioCam HRm	Zeiss		
other	40x / 1.2 NA water immersion objective	Zeiss		
other	20x / 0.8 NA objective	Zeiss		

other	M165FC	Leica		
other	Achromat 1.6x objective	Leica		
other	GFP Filter set ET470/40x; ET525/50m	Leica		
other	mCherry Filter set ET560/40x; ET630/75m	Leica		
other	pco.edge 4.2 bi sCMOS	PCO		
other	Cell Center Stockroom (Penn)	other	RRID:SCR_022399	
other	CDB Microscopy Core (Penn)	other	RRID:SCR_022373	